
Learning to Reduce Search Space for Generalizable Neural Routing Solver

Changliang Zhou^{1,2*} **Xi Lin**^{3*} **Zhenkun Wang**^{1,2,4†} **Qingfu Zhang**³

¹ School of Automation and Intelligent Manufacturing,

Southern University of Science and Technology, Shenzhen, China

² Guangdong Provincial Key Laboratory of Fully Actuated System Control Theory and Technology,

Southern University of Science and Technology, Shenzhen, China

³ Department of Computer Science,

City University of Hong Kong, Hong Kong SAR, China

⁴ Department of Computer Science and Engineering,

Southern University of Science and Technology, Shenzhen, China

zhoucl2022@mail.sustech.edu.cn, xi.lin@my.cityu.edu.hk,

wangzhenkun90@gmail.com, qingfu.zhang@cityu.edu.hk

Abstract

Constructive neural combinatorial optimization (NCO) has attracted growing research attention due to its ability to solve complex routing problems without relying on handcrafted rules. However, existing NCO methods face significant challenges in generalizing to large-scale problems due to high computational complexity and inefficient capture of structural patterns. To address this issue, we propose a novel learning-based search space reduction method that adaptively selects a small set of promising candidate nodes at each step of the constructive NCO process. Unlike traditional methods that rely on fixed heuristics, our selection model dynamically prioritizes nodes based on learned patterns, significantly reducing the search space while maintaining solution quality. Experimental results demonstrate that our method, trained solely on 100-node instances from uniform distribution, generalizes remarkably well to large-scale Traveling Salesman Problem (TSP) and Capacitated Vehicle Routing Problem (CVRP) instances with up to 1 million nodes from the uniform distribution and over 80K nodes from other distributions.

1 Introduction

The Vehicle Routing Problem (VRP) is one of the core problems in Operations Research with significant practical implications in domains such as logistics, supply chain management, and express delivery [1, 2]. Efficient routing optimization is crucial for enhancing delivery performance and reducing operational costs. Traditional heuristic algorithms, such as LKH3 [3] and HGS [4], have demonstrated strong capabilities in solving VRPs with diverse constraints. However, these methods face two fundamental limitations: (1) their design requires extensive domain expertise to craft problem-specific rules, and (2) their computational complexity scales poorly with instance size due to the NP-hard nature of VRPs. These challenges are particularly acute for large-scale instances (e.g., more than 10,000 nodes), where existing algorithms often fail to provide practical solutions with a reasonable runtime.

In recent years, neural combinatorial optimization (NCO) has emerged as a promising paradigm for solving complex problems like VRPs, which eliminates the need for time-consuming and handcrafted

*Equal contribution

†Corresponding author

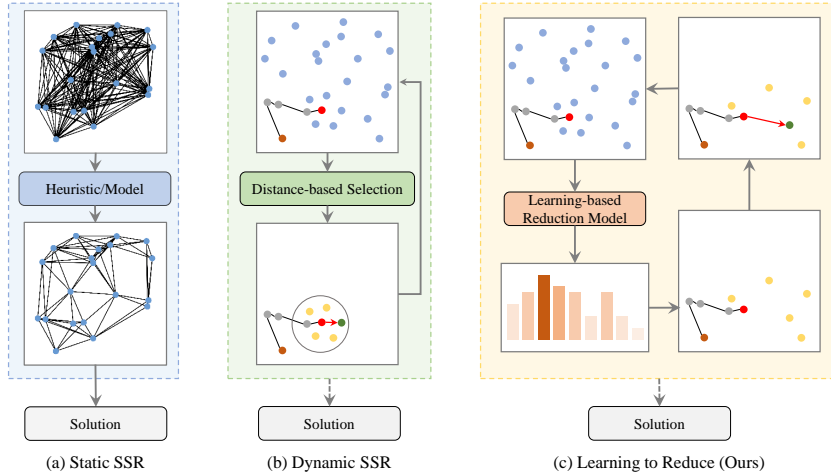


Figure 1: **Different Search Space Reduction (SSR) Methods:** (a) **Static Search Space Reduction** prunes the whole search space only once at the beginning of optimization process; (b) **Dynamic Search Space Reduction** reduces the search space to a small set of candidate nodes based on the distance to the last visited node at each construction step; (c) **Learning to Reduce (Ours)** builds reinforcement learning based model to adaptively reduce the search space and then select the next node for solution construction.

algorithm design by experts [5, 6, 7]. These methods automatically learn problem-specific patterns through training frameworks such as supervised learning (SL) [8, 9, 10, 11, 12, 13] or reinforcement learning (RL) [14, 15, 16, 17]. A well-trained NCO model can directly construct approximate solutions without explicit search, offering a promising direction for real-time VRP solving. However, SL-based methods face a critical limitation due to the difficulty of obtaining high-quality labeled data (e.g., nearly optimal solutions) for large-scale NP-hard problems. In contrast, RL-based methods do not require labeled data and have demonstrated strong performance on small-scale instances (e.g., 100 nodes) [18, 19, 20]. Nevertheless, their effectiveness diminishes significantly on large-scale instances (e.g., 10,000 nodes), primarily due to the exponentially growing search space and the challenge of sparse reward.

To address the scalability challenges, search space reduction (SSR) has gained increasing attention as a scalable strategy. As listed in Table 1, existing SSR techniques can be broadly categorized into two types: static and dynamic. Static SSR performs a one-time pruning at the beginning of the optimization process, offering computational efficiency. However, it often requires additional search procedures (e.g., Monte Carlo Tree Search for TSP) to achieve high-quality solutions [22, 23, 24]. In contrast, dynamic SSR [28, 26, 27] adaptively adjusts the candidate node set at each construction step based on real-time problem states, enabling more effective search space reduction for constructive NCO methods. Despite their advantages, existing dynamic SSR methods are fundamentally constrained by their reliance on distance-based node selection, which struggle to generalize to large-scale instances, particularly those with non-uniform node distributions. We provide a comprehensive literature review of search space reduction approaches in Appendix B.

Table 1: Comparison between our L2R and classical neural vehicle routing solvers with search space reduction.

Neural Routing Solver	Static SSR	Dynamic SSR	Training Scale	Generalizable Scale
MLPR [21]	✓	✗	100	2K
Att-GCN+MCTS [22]	✓	✗	50	10K
DIMES [23]	✓	✗	10K	10K
DIFUSCO [24]	✓	✗	10K	10K
T2T [25]	✓	✗	1K	1K
BQ [10]‡	✗	Distance-based	100	1K
ELG [26]	✗	Distance-based	100	7K
DAR [27]	✗	Distance-based	500	11K
INVIT [28]	✗	Distance-based	100	10K
L2R (Ours)	✓	Learning-based	100	1M

‡ BQ [10] limits the sub-graph to the 250 nearest neighbors of the current node when facing large-scale instances.

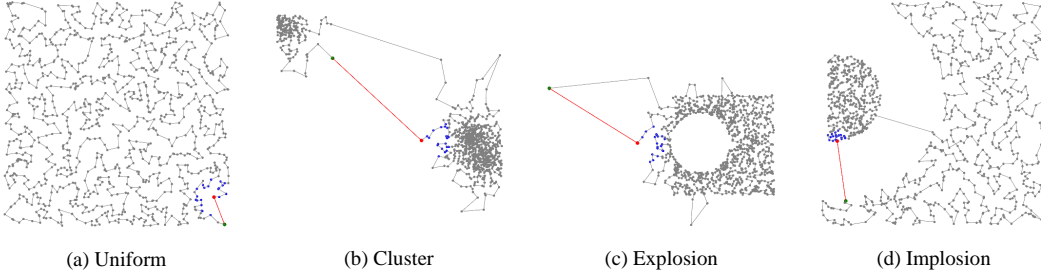


Figure 2: **Impacts of distance-based search space reduction on solution optimality.** (a)-(d) Optimal solutions for TSP1K instances under four distribution patterns: uniform, cluster, explosion, and implosion. Restricting the search space to the k -nearest neighbors ($k = 20$) will lead to suboptimal routes. The red, green, and blue nodes indicate the current node, the next visiting node, and k nearest neighbors, respectively.

As shown in Figure 1, unlike existing SSR approaches, this work proposes a novel *Learning to Reduce (L2R)* framework for more flexible search space reduction that does not rely on the distance between nodes. Our contributions can be summarized as follows:

- We comprehensively analyze the key limitations of existing distance-based SSR methods and then propose a novel learning-based framework with hierarchical static and dynamic SSR for solving large-scale VRPs.
- In particular, we develop an RL-based approach to reduce the search space and select candidate nodes at each construction step, significantly reducing computational overhead without compromising solution quality.
- We conduct comprehensive experiments to demonstrate that our proposed method, trained only on 100-node instances from uniform distribution, can generalize remarkably well to instances with up to 1 million nodes from uniform distribution and over 80k nodes from other distributions.

2 Shortcomings of Distance-based Search Space Reduction

The fundamental limitation of distance-based search space reduction lies in its tendency to prune globally optimal nodes during solution generation. As demonstrated in Figure 2, restricting candidate nodes to the k -nearest neighbors forces the algorithm to ignore critical long-range connections necessary for optimal routing. This over-pruning effect accumulates systematically throughout the solving process, ultimately compromising solution quality. In this section, we systematically analyze these shortcomings through the impact on the optimality gap of the classic solver and the impact on constructive NCO methods across diverse architectures.

Impact on Optimality Gap To evaluate the impact of distance-based search space reduction on final optimization performance, we adopt the widely-used LKH-3 algorithm [3] as our benchmark solver and conduct experiments on the TSPLIB dataset [29]. Given that LKH-3 is not a constructive heuristic, we restrict the search space for each instance by pruning the original fully connected graph into a sparse topology. Specifically, only connections to the k nearest nodes are retained for each node in our experiments.

The results in Table 2 illustrate the performance across TSPLIB instances of varying scales under

Table 2: Optimality gap comparison of LKH-3 on unreduced and reduced TSPLIB instances.

Instance	Scale	w/o D-SSR	w/ $k = 10$	w/ $k = 20$
dsj1000	1,000	0.00%	7.27%	6.85%
pr1002	1,002	0.00%	3.14%	1.06%
d1291	1,291	0.00%	26.71%	9.59%
fl1400	1,400	0.02%	64.72%	54.29%
fl1577	1,577	0.01%	48.14%	38.19%
d1655	1,655	0.00%	20.41%	8.74%
rl1889	1,889	0.00%	27.94%	8.45%
d2103	2,103	0.01%	17.62%	6.10%
fl3795	3795	0.06%	56.87%	53.38%
rl5915	5,915	0.03%	17.99%	2.58%
rl5934	5,934	0.03%	27.24%	6.40%
rl11849	11,849	0.00%	11.01%	1.90%
usa13509	13,509	0.01%	20.06%	5.87%
Avg.gap		0.01%	26.86%	15.64%

different levels of search space reduction (k). A key observation is that while LKH-3 achieves near-optimal solutions in an unreduced search space, aggressive pruning (i.e., using small k values) substantially degrades performance. This degradation is particularly pronounced in instances where optimal routes inherently depend on non-local node selections, which may be eliminated by such aggressive pruning strategies. We provide detailed solution visualizations comparing three different results in Appendix C.1.

Impact on Constructive NCOs For constructive NCO methods, each construction step should consider all feasible nodes to guarantee optimality. However, since VRPs are classic NP-hard problems, the computational complexity grows exponentially with problem size. For large-scale instances, directly obtaining high-quality solutions remains extremely challenging in an unreduced search space. While distance-based SSR methods [10, 28] improve computational efficiency, they also introduce critical limitations in their failure to include a small but essential subset of nodes within their candidate set. The experimental results shown in Appendix C.2 highlight the potential of search space reduction while underscoring the need for advanced reduction methods capable of efficiently handling large-scale problems with a small k .

3 Learning to Reduce (L2R)

In this section, we propose *Learning to Reduce (L2R)*, a hierarchical neural framework to address the scalability limitations of search space reduction in vehicle routing problems. As illustrated in Figure 3, our framework introduces three complementary stages: 1) static reduction, 2) learning-based reduction, and 3) local solution construction.

3.1 Static Reduction

The static reduction stage initiates our hierarchical framework by pruning the original fully connected graph $G = (\Omega, E)$ into a sparse topology $G' = (\Omega, E')$. For each node $i \in \Omega$, we compute pairwise Euclidean distances $\{d_{ij}\}_{j=1}^N$ and eliminate connections to nodes in the farthest γ -percentile. Formally, the sparse edge set is defined as

$$E' = \bigcup_{i \in \Omega} \{e_{ij} \mid \text{rank}(d_{ij}) \leq (1 - \gamma)|\Omega|\}, \quad \alpha \in [0, 1] \quad (1)$$

where $\text{rank}(d_{ij})$ denotes the ascending order of distances from v_i (i.e., $\text{rank}(d_{ij}) = 1$ for the closest neighbor). Through empirical analysis across diverse scales and node distributions, we use $\gamma = 10\%$ as the threshold in this work, which can efficiently reduce the computational overhead without compromising solution optimality. Crucially, this stage operates as a one-time preprocessing step, incurring no runtime overhead during subsequent solving phases.

3.2 Learning-based Reduction

The static reduction stage conducts partial search space pruning. However, there is still a large number of non-optimal edges remaining in the pruned graph G' , which imposes prohibitive computational costs for NCO in large-scale scenarios. However, as discussed in the previous section, further distance-based search reduction with a large reduced rate will lead to a poor optimality ratio and poor performance.

To mitigate the negative impact of reduction on optimality, we develop a learning-based model to dynamically evaluate the potential of feasible nodes and adaptively reduce the search space at each construction step. Our proposed model ensures efficiency through a lightweight structure containing only an embedding layer and an attention layer. Their implementations are detailed in the following.

Embedding Layer Given an instance $S = \{\mathbf{s}_i\}_{i=1}^n$ with n node features $\mathbf{s}_i \in \mathbb{R}^{d_x}$ (e.g., city coordinates in TSP), we first project these features into d -dimensional embeddings through a shared linear transformation for each node:

$$\mathbf{h}_i^D = W^{(e)} \mathbf{s}_i + \mathbf{b}^{(e)}, \quad \forall i \in \{1, \dots, N\} \quad (2)$$

where $W^{(e)} \in \mathbb{R}^{d_x \times d}$ and $\mathbf{b}^{(e)} \in \mathbb{R}^d$ are learnable parameters. In other words, we obtain a set of embeddings $H^D = \{\mathbf{h}_i^D\}_{i=1}^n \in \mathbb{R}^{n \times d}$ for all nodes in the instance S .

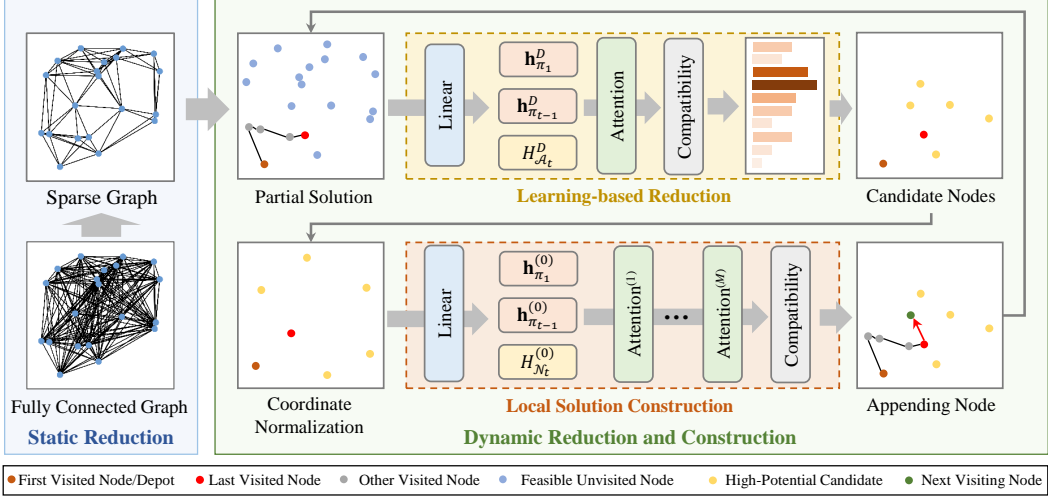


Figure 3: The pipeline of our proposed L2R framework for solving large-scale vehicle routing problem instances.

At t -th step with partial solution $(\pi_1, \dots, \pi_{t-1})$, we adopt the setting from Kool et al. [16] to represent the current partial solution using the initial node embedding $\mathbf{h}_{\pi_1}^D$ and latest node embedding $\mathbf{h}_{\pi_{t-1}}^D$. In addition, following Kwon et al. [18], we define a context embedding of the current partial solution:

$$\mathbf{h}_{CD}^t = W_{\text{first}} \mathbf{h}_{\pi_1}^D + W_{\text{last}} \mathbf{h}_{\pi_{t-1}}^D, \quad (3)$$

where $W_{\text{first}} \in \mathbb{R}^{d \times d}$ and $W_{\text{last}} \in \mathbb{R}^{d \times d}$ are two learnable matrices. In addition, we denote \mathcal{A}_t as the set of all feasible nodes (e.g., unvisited cities with a valid edge in E' connected to the current city) at the t -th step. The embeddings of \mathcal{A}_t are denoted by $H_{\mathcal{A}_t}^D = \{\mathbf{h}_i^D | i \in \mathcal{A}_t\} \in \mathbb{R}^{|\mathcal{A}_t| \times d}$.

Attention Layer To calculate potential scores for all feasible nodes in \mathcal{A}_t , we process the context embedding \mathbf{h}_{CD}^t and node embeddings $H_{\mathcal{A}_t}^D$ through an attention mechanism. First, we project the node embeddings into key-value pairs:

$$K_{\mathcal{A}_t}^D = W^K H_{\mathcal{A}_t}^D, \quad V_{\mathcal{A}_t}^D = W^V H_{\mathcal{A}_t}^D \quad (4)$$

where $W^K, W^V \in \mathbb{R}^{d \times d}$ are learnable projection matrices. The context embedding \mathbf{h}_{CD}^t then interacts with these projections through the attention operator:

$$\hat{\mathbf{h}}_{CD}^t = \text{Attention}(\mathbf{h}_{CD}^t, K_{\mathcal{A}_t}^D, V_{\mathcal{A}_t}^D) \quad (5)$$

Compatibility Calculation Finally, similar to previous work [16, 18, 17], we can compute the compatibilities $\mathbf{u}^R = \{u_{t,i}^R | i \in \mathcal{A}_t\}$ for selecting each node in \mathcal{A}_t :

$$u_{t,i}^R = \begin{cases} \xi \cdot \tanh\left(\frac{\hat{\mathbf{h}}_{CD}^t (\mathbf{h}_i^D)^T}{\sqrt{d_k}} + a_{t-1,i}^R\right) & \text{if } i \in \mathcal{A}_t \\ -\infty & \text{otherwise} \end{cases}, \quad (6)$$

where ξ is the clipping parameter, d_k is the dimension for matrix $K_{\mathcal{A}_t}^D$, and $a_{t-1,i}^R$ is the adaptation bias between each node $i \in \mathcal{A}_t$ and the current node π_{t-1} , following Zhou et al. [17] (see Appendix D for more details). Finally, the potential scores $\mathbf{o} = \{o_i | i \in \mathcal{A}_t\} \in \mathbb{R}^{1 \times |\mathcal{A}_t|}$ can be computed as:

$$\mathbf{o} = \text{softmax}(\mathbf{u}^R). \quad (7)$$

The score o_i quantifies the potential of node $i \in \mathcal{A}_t$. Then, we retain the top- k nodes with the highest potential scores as the candidate nodes and denote the set of all candidate nodes as \mathcal{N}_t . In this way, we conduct a learning-based dynamic search space reduction at each construction step. More details about search space reduction for CVRPs can be found in Appendix E.

3.3 Local Solution Construction

In this subsection, we develop a learning-based local solution construction model to select one final node from the candidate set \mathcal{N}_t to construct the partial solution at construction step t . Similar to previous work [16, 18, 10, 9], we also use the initial node π_1 and the latest node π_{t-1} to represent the current partial solution. First of all, the embedding of each node can be obtained by a shared linear transformation:

$$\mathbf{h}_i^{(0)} = W^{(0)} \mathbf{s}_i + \mathbf{b}^{(0)}, \quad \forall i \in \{\pi_1, \pi_{t-1}\} \cup \mathcal{N}_t \quad (8)$$

where $W^{(0)}$ and $\mathbf{b}^{(0)}$ are learnable parameters. Then we obtain the embedding of the partial graph:

$$\tilde{H}^{(0)} = [W_1 \mathbf{h}_{\pi_1}^{(0)}, W_2 \mathbf{h}_{\pi_{t-1}}^{(0)}, H_{\mathcal{N}_t}^{(0)}] \in \mathbb{R}^{(2+|\mathcal{N}_t|) \times d} \quad (9)$$

where $[\cdot, \cdot]$ denotes the vertical concatenation operator, $H_{\mathcal{N}_t}^{(0)} = \{\mathbf{h}_i^{(0)} | i \in \mathcal{N}_t\} \in \mathbb{R}^{|\mathcal{N}_t| \times d}$ are the embeddings for all candidate nodes in \mathcal{N}_t , $W_1 \in \mathbb{R}^{d \times d}$ and $W_2 \in \mathbb{R}^{d \times d}$ are two learnable matrices. This embedding is the initial input to a sequence of attention layers.

In our proposed local solution construction model, one attention layer consists of two sub-layers: an attention sub-layer and a Feed-Forward (FF) sub-layer, both of which use Layer Normalization [30] and skip-connection [31]. The detailed process can be found in Appendix F.3. After M attention layers, the final embedding $\tilde{H}^{(M)} = [\mathbf{h}_{\pi_1}^{(M)}, \mathbf{h}_{\pi_{t-1}}^{(M)}, H_{\mathcal{N}_t}^{(M)}] \in \mathbb{R}^{(2+|\mathcal{N}_t|) \times d}$ contains advanced feature representations of the initial, last, and k candidate nodes.

Finally, we compute the probabilities for selecting each node in \mathcal{N}_t via another compatibility module different from Equation (6):

$$u_{t,i}^L = \begin{cases} \xi \cdot \tanh \left(\frac{\hat{\mathbf{h}}_{(C)}^t (\mathbf{h}_i^{(M)})^T}{\sqrt{d_k}} + a_{t-1,i}^L \right) & \text{if } i \in \mathcal{N}_t \\ -\infty & \text{otherwise} \end{cases}, \quad (10)$$

where $\hat{\mathbf{h}}_{(C)}^t = \mathbf{h}_{\pi_1}^{(M)} + \mathbf{h}_{\pi_{t-1}}^{(M)}$ and $a_{t-1,i}^L$ represents the adaptation bias between each node $i \in \mathcal{N}_t$ and π_{t-1} . The probabilities $\mathbf{p} = \{p_i | i \in \mathcal{N}_t\}$ of selecting the candidate node i can be calculated as

$$\mathbf{p} = \text{softmax}(\mathbf{u}^L). \quad (11)$$

More details of the local solution construction model are provided in Appendix F.

3.4 Training

Our proposed L2R framework has a learning-based reduction model and a local solution construction model, which can be trained by a joint training scheme. We denote the learnable parameters as $\boldsymbol{\theta}_R$ and $\boldsymbol{\theta}_L$ for the reduction model and local solution construction model, respectively. Hence $\boldsymbol{\theta} = \{\boldsymbol{\theta}_R, \boldsymbol{\theta}_L\}$ contains all learnable parameters in the L2R framework.

L2R samples the node π_t by probabilities $\mathbf{p} = \{p_i | i \in \mathcal{N}_t\}$ and add it to current partial solution, a complete solution $\pi = (\pi_1, \dots, \pi_n)$ for an instance S is constructed by $\boldsymbol{\theta}_L$ with n decoding steps. Since the reduction model is only responsible for selecting k candidate nodes and does not participate in the actual node selection process, we use the total reward $\mathcal{R}(\pi | S, \boldsymbol{\theta}_L)$ (e.g., the negative value of tour length) of instance S given a specific solution π generated by $\boldsymbol{\theta}_L$ for the training of both $\boldsymbol{\theta}_R$ and $\boldsymbol{\theta}_L$ simultaneously, and we define $\tau = (\tau_1, \dots, \tau_n)$ as the set of sampled nodes by $\boldsymbol{\theta}_R$. Following previous NCO works [16, 28, 32], L2R is trained by the REINFORCE [33] gradient estimator:

$$\mathcal{L}_{\text{Joint}}(\boldsymbol{\theta}) = \mathcal{L}_R(\boldsymbol{\theta}_R) + \mathcal{L}_L(\boldsymbol{\theta}_L), \quad (12)$$

$$\nabla_{\boldsymbol{\theta}_R} \mathcal{L}_R(\boldsymbol{\theta}_R) = \mathbb{E}_{o(\tau|S, \boldsymbol{\theta}_R)} [(\mathcal{R}(\pi|S, \boldsymbol{\theta}_L) - b(S)) \nabla_{\boldsymbol{\theta}_R} \log o(\tau|S)], \quad (13)$$

$$\nabla_{\boldsymbol{\theta}_L} \mathcal{L}_L(\boldsymbol{\theta}_L) = \mathbb{E}_{p(\pi|S, \boldsymbol{\theta}_L)} [(\mathcal{R}(\pi|S, \boldsymbol{\theta}_L) - b(S)) \nabla_{\boldsymbol{\theta}_L} \log p(\pi|S)], \quad (14)$$

where $o(\tau | S) = \prod_{t=2}^n o(\tau_t | S, \pi_{1:t-1})$, $p(\pi | S) = \prod_{t=2}^n p(\pi_t | S, \pi_{1:t-1})$, $b(S)$ is the greedy rollout baseline. The detailed training process is provided in Appendix H.

4 Experiments

In this section, we comprehensively evaluate our proposed model against classical and learning-based solvers on synthetic and real-world TSP and CVRP instances³. Notably, our model is trained solely on 100-node TSP instances from uniform distribution. We assess its generalization performance on: (1) scalability to problem sizes up to 1 million nodes and (2) robustness to varying node distributions.

4.1 Experimental Setup

Problem Setting For all problems, we generate synthetic instances following the methodology outlined in Kool et al. [16]. Specifically, we construct TSP test datasets with uniformly distributed nodes at six scales: 1K, 5K, 10K, 50K, 100K, and 1M. Following Fu et al. [22], the TSP1K test set consists of 128 instances, while the larger TSP datasets each contain 16 instances. For the CVRP, we adhere to the capacity constraints specified in Hou et al. [34] and generate five test datasets with scales of 1K, 5K, 7K, 10K, and 1M. Each dataset includes 100 instances, except for CVRP10K and CVRP1M, which contain 16 instances.

The optimal solutions for the TSP and CVRP instances are obtained using LKH3 [3] and HGS [4], respectively. To evaluate cross-distribution generalization performance, we test on the TSP/CVRP5K instances obtained from INVIT [28]. Additionally, we validate the real-world performance of L2R using symmetric EUC_2D instances from TSPLIB [29] and CVRPLIB Set-XXL [35].

Model & Training Setting For all experiments, we use an embedding dimension of 128 and a feed-forward layer dimension of 512. To enhance geometric pattern recognition in VRPs, we integrate scale and distance information into the attention mechanism (see Appendix G for implementation details). The local construction model employs 6 attention layers. Consistent with Kool et al. [16], we set the clipping parameter $\xi = 10$ in Equation (6) and Equation (10). The hyperparameter k is configured as 20 for TSP and 50 for CVRP. All experiments are conducted on a single NVIDIA GeForce RTX 3090 GPU (24GB memory).

Our model is exclusively trained on uniformly distributed instances with 100 nodes. We employ the Adam optimizer [36] with an initial learning rate of $\eta = 10^{-4}$ and a learning rate decay of 0.98 per epoch. Training spans 100 epochs with 2,500 batches per epoch. Due to memory constraints, batch sizes differ across problems—180 for TSP and 60 for CVRP. The same pre-trained model is used in all experimental evaluations for each problem. Additional implementation details are provided in Appendix H (pseudocode for training) and Appendix I (training and model settings).

Baseline We compare L2R with the following methods: (1) **Classical Solver**: Concorde [37], LKH3 [3], HGS [4]; (2) **Constructive NCO**: POMO [18], Omni_VRP [38], ELG [26], BQ [10], LEHD [9], and INVIT [28]; (3) **Two-Stage NCO**: TAM [34] and GLOP [39].

Metrics and Inference We report the average objective value (Obj.), optimality gap (Gap), and average inference time (Time) for each method. The optimality gap quantifies the discrepancy between the solutions generated by the corresponding methods and the optimal solutions. It is important to note that the inference time for classical solvers, which run on a single CPU, and for learning-based methods, which utilize GPUs, are inherently different. Therefore, these times should not be directly compared.

For most NCO baseline methods, we execute the source code provided by the authors using default settings. Results marked with an asterisk (*) are directly obtained from the corresponding papers. Some methods fail to produce feasible solutions within a reasonable time limit (e.g., several days), which is denoted by ‘N/A’. The notation ‘OOM’ indicates that the memory consumption exceeds the available memory limits. For L2R, we report two types of results, which are obtained by greedy trajectory (greedy) and those derived from Parallel local ReConstruction (PRC) under different numbers of iterations [40]. The parallel approach demonstrates promising results by effectively trading computing time for improved solution quality. For PRC, initial solutions are generated using the greedy trajectory. PRC100 refers to 100 iterations, with the longest destruction length per iteration set to 1,000 to balance speed and effectiveness. Further details about PRC are available in [40].

³We provide detailed definitions and formulations of TSP and CVRP in Appendix A.

Table 3: Comparison on TSP instances with uniform distribution.

Method	TSP1K		TSP5K		TSP10K		TSP50K		TSP100K	
	Obj. (Gap)	Time	Obj. (Gap)	Time	Obj. (Gap)	Time	Obj. (Gap)	Time	Obj. (Gap)	Time
LKH3	23.12 (0.00%)	1.7m	50.97 (0.00%)	12m	71.78 (0.00%)	33m	159.93 (0.00%)	10h	225.99 (0.00%)	25h
Concorde	23.12 (0.00%)	1m	50.95 (-0.05%)	31m	72.00 (0.15%)	1.4h	N/A	N/A	N/A	N/A
GLOP (more revisions)	23.78 (2.85%)	10.2s	53.15 (4.26%)	1.0m	75.04 (4.39%)	1.9m	168.09 (5.10%)	1.5m	237.61 (5.14%)	3.9m
LEHD greedy	23.84 (3.11%)	0.8s	58.85 (15.46%)	1.5m	91.33 (27.24%)	11.7m	OOM		OOM	
LEHD RRC1,000	23.29 (0.72%)	3.3m	54.43 (6.79%)	8.6m	80.90 (12.5%)	18.6m	OOM		OOM	
BQ greedy	23.65 (2.30%)	0.9s	58.27 (14.31%)	22.5s	89.73 (25.02%)	1.0m	OOM		OOM	
BQ bs16	23.43 (1.37%)	13s	58.27 (10.7%)	24s	OOM		OOM		OOM	
POMO aug \times 8	32.51 (40.6%)	4.1s	87.72 (72.1%)	8.6m	OOM		OOM		OOM	
ELG aug \times 8	25.74 (11.33%)	0.8s	60.19 (18.08%)	21s	OOM		OOM		OOM	
INVIT-3V greedy	24.67 (6.71%)	0.4s	54.46 (6.84%)	12.7s	76.87 (7.09%)	34.9s	171.42 (7.18%)	4.9m	242.26 (7.20%)	18.8m
L2R greedy	24.16 (4.49%)	0.05s	53.36 (4.69%)	1.8s	75.24 (4.82%)	4.1s	167.70 (4.86%)	35.5s	236.81 (4.79%)	1.8m
L2R PRC100	23.62 (2.18%)	2.5s	52.41 (2.82%)	20.1s	73.95 (3.03%)	26.3s	165.16 (3.27%)	1.8m	234.36 (3.70%)	3.2m
L2R PRC500	23.54 (1.82%)	12.6s	52.25 (2.50%)	1.6m	73.73 (2.72%)	2.0m	164.61 (2.92%)	6.6m	233.24 (3.21%)	8.8m
L2R PRC1,000	23.52 (1.72%)	24.9s	52.20 (2.40%)	3.1m	73.66 (2.62%)	3.8m	164.41 (2.80%)	12.4m	232.77 (3.00%)	15.5m

4.2 Performance Evaluation

Cross-Size Generalization

We conduct experiments on large-scale routing instances with uniform distribution, and the experimental results are reported in Table 3 (TSP1K–TSP100K), Table 4 (CVRP1K–CVRP10K), and Table 5 (TSP/CVRP1M). Benefiting from an efficient search space reduction scheme, our method consistently delivers superior inference performance across various problem instances. While it does not surpass SL-based LEHD and BQ on TSP/CVRP1K, RL-based L2R

achieves shorter runtime compared to other methods, such as LEHD (e.g., 25 sec vs. 3.3 min on TSP1K instances), and L2R can outperform all comparable RL-based methods. For larger-scale instances, our proposed L2R, trained only on 100-node instances, significantly improves the scalability of NCO methods and outperforms other methods (including BQ and LEHD). To the best of our knowledge, L2R is the first neural solver capable of effectively solving TSP and CVRP instances with one million nodes. Compared to classic heuristic methods, L2R achieves a 4.79% optimality gap and a 4 \times speed-up over LKH-3 on 16 TSP1M instances. Additionally, L2R successfully tackles CVRP1M instances that exceed the computational limits of both LKH3 and HGS.

Cross-Distribution Generalization We evaluate the cross-distribution performance of L2R on TSP5K/CVRP5K instances from three distinct distributions: cluster, explosion, and implosion. As shown in Table 6, L2R consistently achieves the best performance among all comparable methods across these distributions. These results further highlight the robust generalization capabilities of our proposed L2R.

Results on Benchmark Dataset We further assess the generalization performance of L2R on instances from CVRPLIB Set-XXL [35] and TSPLIB [29]. As demonstrated in Table 7, L2R maintains its position as the best-performing model across instances of varying scales, underscoring its practical applicability in real-world scenarios. Detailed results are provided in Appendix J.

Table 4: Comparison on CVRP instances following the setting in Hou et al. [34].

Method	CVRP1K		CVRP5K		CVRP7K		CVRP10K	
	Obj. (Time)	Time	Obj. (Time)	Time	Obj. (Time)	Time	Obj. (Time)	Time
HGS	41.2 (5m)		126.2 (5m)		172.1 (5m)		227.2 (5m)	
TAM-HGS*	—		142.8 (30s)		193.6 (52s)		—	
GLOP-G (LKH-3)	45.9 (1.1s)		140.6 (4.0s)		191.2 (5.8s)		256.4 (6.2s)	
LEHD greedy	44.0 (0.8s)		138.2 (1.4m)		189.5 (3.8m)		257.3 (12m)	
LEHD RRC1000	42.4 (3.4m)		132.7 (10m)		180.6 (19m)		243.8 (51.6m)	
BQ greedy	44.2 (1s)		139.9 (18.5s)		192.3 (42.2s)		262.2 (2m)	
BQ bs16	43.1 (14s)		136.4 (2.4m)		186.8 (5.7m)		OOM	
POMO aug \times 8	101.0 (4.6s)		632.9 (11m)		OOM		OOM	
ELG aug \times 8	46.4 (10.3s)		OOM		OOM		OOM	
INVIT-3V greedy	48.3 (1s)		146.2 (7s)		197.3 (11s)		262.5 (1.2m)	
L2R greedy	45.8 (0.1s)		136.0 (0.5s)		180.5 (0.8s)		236.7 (4.4s)	
L2R PRC100	44.7 (4.0s)		132.7 (14.4s)		177.2 (19.8s)		233.2 (39.9s)	
L2R PRC500	44.4 (20.0s)		131.2 (1.2m)		175.5 (1.6m)		230.9 (3.0m)	
L2R PRC1,000	44.3 (40.3s)		130.6 (2.3m)		174.7 (3.2m)		230.1 (6.0m)	

Table 5: Comparison of TSP and CVRP instances with one million nodes.

Method	TSP1M		CVRP1M		
	Obj.	Gap	Obj.	Gap	
Concorde	N/A	N/A	N/A	—	
HGS	—	—	—	—	
LKH3	713.97	0.00%	4.8h	N/A	
POMO		OOM		OOM	
ELG		OOM		OOM	
INVIT-3V greedy	N/A	N/A	N/A	N/A	
L2R greedy	748.18	4.79%	1.2h	17231.85	0.00%

Table 6: Comparison on cross-distribution generalization.

Method	TSP5K, Cluster Gap	Time	TSP5K, Explosion Gap	Time	TSP5K, Implosion Gap	Time	CVRP5K, Cluster Gap	Time	CVRP5K, Explosion Gap	Time	CVRP5K, Implosion Gap	Time
Optimal	0.00%	—	0.00%	—	0.00%	—	0.00%	—	0.00%	—	0.00%	—
ELG multi-greedy [‡]	22.83%	1.6m	20.71%	1.6m	17.55%	1.6m	18.14%	2.4m	13.21%	2.2m	7.50%	2.2m
Omni_VRP multi-greedy [‡]	54.53%	1.1m	51.09%	1.1m	50.20%	1.1m	22.05%	1.3m	33.09%	1.4m	40.20%	1.3m
INVIT-3V greedy	8.20%	11.3s	11.48%	11.3s	8.52%	11.3s	9.05%	29.4s	8.44%	29.3s	8.77%	23.2s
L2R greedy	6.14%	1.5s	9.54%	1.5s	6.17%	1.5s	2.65%	1.8s	4.38%	1.8s	3.15%	1.8s
L2R PRC1,000	3.16%	2.6m	3.52%	2.6m	2.87%	2.6m	0.99%	4.2m	1.14%	4.2m	0.73%	4.2m

[†] All datasets are obtained from INVIT[28] and each contains 20 instances.

[‡] The instance augmentation technique is not employed for comparable methods to prevent methods from exceeding memory limits.

Table 7: Comparison on large-scale TSPLIB [29] instances ($5,000 \leq N \leq 85,900$) and CVRPLIB [35] instances ($3,000 \leq N \leq 30,000$).

Method	TSPLIB				CVRPLIB-XXL			
	$1K \leq N \leq 5K$ (23 instances)	$5K < N \leq 100K$ (10 instances)	All (33 instances)	Solved#	$3K \leq N \leq 7K$ (4 instances)	$7K < N \leq 30K$ (6 instances)	All (10 instances)	Solved#
GLOP	6.16%	7.69%	6.62%	33/33	17.07%	21.32%	19.62%	10/10
TAM-LKH3*	—	—	—	—	20.44%	—	—	—
BQ bs16	10.65%	30.58% [†]	—	26/33	20.20%	OOM	—	4/10
LEHD greedy	11.14%	39.34% [†]	—	30/33	22.22%	32.80% [†]	—	6/10
LEHD RRC1000	4.00%	18.46% [†]	—	30/33	14.06%	21.52% [†]	—	6/10
POMO aug $\times 8$	62.81%	OOM	—	23/33	331.24% [†]	OOM	—	2/10
ELG aug $\times 8$	11.34%	OOM	—	23/33	16.82% [†]	OOM	—	2/10
INVIT-3V greedy	11.49%	10.03%	11.05%	33/33	20.74%	26.64%	24.28%	10/10
L2R greedy	9.16%	7.36%	8.61%	33/33	12.05%	11.22%	11.55%	10/10
L2R PRC100	3.60%	4.58%	3.89%	33/33	8.62%	9.34%	9.05%	10/10

[†] Some instances are skipped due to the OOM issue.

4.3 Additional Analyses

L2R vs. D-SSR To validate the effectiveness of our proposed L2R, we conduct a comparative experiment against a dynamic distance-based SSR model, ensuring identical experimental settings. We systematically analyze the advantages of L2R, mainly including: (1) overall performance on real-world instances, (2) optimality gap and optimality ratio per instance, (3) impacts of different candidate node selection strategies, and (4) solution visualizations comparing the two approaches. As detailed in Appendix K.1, L2R consistently demonstrates better candidate selection on real-world problems and significantly outperforms the dynamic D-SSR baseline. These findings further underscore the superior practical applicability of L2R in real-world scenarios.

Complexity Analysis We present the time and space complexity analyses for three different constructive models: L2R with learning-based SSR, INVIT with distance-based SSR, and LEHD without SSR. The results in Appendix K.2 demonstrate that our local solution construction model achieves significantly lower computational complexity than both LEHD and INVIT. This advantage is particularly evident in the substantially reduced runtime compared to existing representative models.

4.4 Ablation Study

We conduct a detailed ablation study and analysis to demonstrate the effectiveness and robustness of L2R, mainly including: (1) **L2R vs. Distance-based SSR with Larger Search Space** (see Appendix L.1); (2) **Effects of Adaptation Bias in Compatibility** (see Appendix L.2); (3) **Comparison between Different Attention Mechanisms** (see Appendix L.3).

5 Conclusion, Limitation, and Future Work

In this work, we propose a novel RL-based Learning-to-Reduce (L2R) framework for solving large-scale vehicle routing problems. Our approach adaptively selects a small set of candidate nodes at each construction step, enabling efficient search space reduction while maintaining solution quality. Extensive experiments demonstrate that L2R, trained exclusively on 100-node instances from the

uniform distribution, achieves remarkable performance on TSP and CVRP instances with up to 1 million nodes from the uniform distribution and over 80K nodes from other distributions.

Limitation and Future Work While L2R achieves impressive performance on large-scale TSP and CVRP instances, it currently relies on a simple combined loss for training. In future work, we aim to develop a more effective loss function to further improve the training efficiency of L2R. In addition, we plan to extend the L2R framework’s applicability to tackle routing problems with complex constraints without compromising solution quality.

References

- [1] Krishna Veer Tiwari and Satyendra Kumar Sharma. An optimization model for vehicle routing problem in last-mile delivery. *Expert Systems with Applications*, 222:119789, 2023.
- [2] Kubra Sar and Pezhman Ghadimi. A systematic literature review of the vehicle routing problem in reverse logistics operations. *Computers & Industrial Engineering*, 177:109011, 2023.
- [3] Keld Helsgaun. An extension of the lin-kernighan-helsgaun tsp solver for constrained traveling salesman and vehicle routing problems. *Roskilde: Roskilde University*, 12, 2017.
- [4] Thibaut Vidal. Hybrid genetic search for the cvrp: Open-source implementation and swap* neighborhood. *Computers & Operations Research*, 140:105643, 2022.
- [5] Yoshua Bengio, Andrea Lodi, and Antoine Prouvost. Machine learning for combinatorial optimization: a methodological tour d’horizon. *European Journal of Operational Research*, 290(2):405–421, 2021.
- [6] Bingjie Li, Guohua Wu, Yongming He, Mingfeng Fan, and Witold Pedrycz. An overview and experimental study of learning-based optimization algorithms for the vehicle routing problem. *IEEE/CAA Journal of Automatica Sinica*, 9(7):1115–1138, 2022.
- [7] Xuan Wu, Di Wang, Lijie Wen, Yubin Xiao, Chunguo Wu, Yuesong Wu, Chaoyu Yu, Douglas L Maskell, and You Zhou. Neural combinatorial optimization algorithms for solving vehicle routing problems: A comprehensive survey with perspectives. *arXiv preprint arXiv:2406.00415*, 2024.
- [8] Oriol Vinyals, Meire Fortunato, and Navdeep Jaitly. Pointer networks. *Advances in Neural Information Processing Systems*, 28, 2015.
- [9] Fu Luo, Xi Lin, Fei Liu, Qingfu Zhang, and Zhenkun Wang. Neural combinatorial optimization with heavy decoder: Toward large scale generalization. In *Thirty-seventh Conference on Neural Information Processing Systems*, 2023.
- [10] Darko Drakulic, Sofia Michel, Florian Mai, Arnaud Sors, and Jean-Marc Andreoli. Bq-nco: Bisimulation quotienting for efficient neural combinatorial optimization. In *Thirty-seventh Conference on Neural Information Processing Systems*, 2023.
- [11] Yubin Xiao, Di Wang, Boyang Li, Mingzhao Wang, Xuan Wu, Changliang Zhou, and You Zhou. Distilling autoregressive models to obtain high-performance non-autoregressive solvers for vehicle routing problems with faster inference speed. In *Proceedings of the AAAI Conference on Artificial Intelligence*, volume 38, pages 20274–20283, 2024.
- [12] Chaitanya K Joshi, Thomas Laurent, and Xavier Bresson. An efficient graph convolutional network technique for the travelling salesman problem. *arXiv preprint arXiv:1906.01227*, 2019.
- [13] Benjamin Hudson, Qingbiao Li, Matthew Malencia, and Amanda Prorok. Graph neural network guided local search for the traveling salesperson problem. In *International Conference on Learning Representations*, 2022.
- [14] Irwan Bello, Hieu Pham, Quoc V Le, Mohammad Norouzi, and Samy Bengio. Neural combinatorial optimization with reinforcement learning. *arXiv preprint arXiv:1611.09940*, 2016.
- [15] Elias Khalil, Hanjun Dai, Yuyu Zhang, Bistra Dilkina, and Le Song. Learning combinatorial optimization algorithms over graphs. *Advances in Neural Information Processing Systems*, 30, 2017.
- [16] Wouter Kool, Herke van Hoof, and Max Welling. Attention, learn to solve routing problems! In *International Conference on Learning Representations*, 2019.
- [17] Changliang Zhou, Xi Lin, Zhenkun Wang, Xialiang Tong, Mingxuan Yuan, and Qingfu Zhang. Instance-conditioned adaptation for large-scale generalization of neural combinatorial optimization. *arXiv preprint arXiv:2405.01906*, 2024.
- [18] Yeong-Dae Kwon, Jinho Choo, Byoungjin Kim, Iljoo Yoon, Youngjune Gwon, and Seungjai Min. Pomo: Policy optimization with multiple optima for reinforcement learning. *Advances in Neural Information Processing Systems*, 33:21188–21198, 2020.

[19] Minsu Kim, Junyoung Park, and Jinkyoo Park. Sym-nco: Leveraging symmetry for neural combinatorial optimization. *Advances in Neural Information Processing Systems*, 35:1936–1949, 2022.

[20] Yubin Xiao, Di Wang, Xuan Wu, Yuesong Wu, Boyang Li, Wei Du, Liupu Wang, and You Zhou. Improving generalization of neural vehicle routing problem solvers through the lens of model architecture. *Neural Networks*, 187:107380, 2025.

[21] Yuan Sun, Andreas Ernst, Xiaodong Li, and Jake Weiner. Generalization of machine learning for problem reduction: a case study on travelling salesman problems. *Or Spectrum*, 43(3):607–633, 2021.

[22] Zhang-Hua Fu, Kai-Bin Qiu, and Hongyuan Zha. Generalize a small pre-trained model to arbitrarily large tsp instances. In *Proceedings of the AAAI Conference on Artificial Intelligence*, volume 35, pages 7474–7482, 2021.

[23] Ruizhong Qiu, Zhiqing Sun, and Yiming Yang. Dimes: A differentiable meta solver for combinatorial optimization problems. *Advances in Neural Information Processing Systems*, 35:25531–25546, 2022.

[24] Zhiqing Sun and Yiming Yang. Difusco: Graph-based diffusion solvers for combinatorial optimization. *Advances in Neural Information Processing Systems*, 36:3706–3731, 2023.

[25] Yang Li, Jinpei Guo, Runzhong Wang, and Junchi Yan. T2t: From distribution learning in training to gradient search in testing for combinatorial optimization. In *Thirty-seventh Conference on Neural Information Processing Systems*, 2023.

[26] Chengrui Gao, Haopu Shang, Ke Xue, Dong Li, and Chao Qian. Towards generalizable neural solvers for vehicle routing problems via ensemble with transferrable local policy. In *International Joint Conference on Artificial Intelligence*, 2024.

[27] Yang Wang, Ya-Hui Jia, Wei-Neng Chen, and Yi Mei. Distance-aware attention reshaping: Enhance generalization of neural solver for large-scale vehicle routing problems. *arXiv preprint arXiv:2401.06979*, 2024.

[28] Han Fang, Zhihao Song, Paul Weng, and Yutong Ban. Invit: A generalizable routing problem solver with invariant nested view transformer. In *International Conference on Machine Learning*, 2024.

[29] Gerhard Reinelt. Tsplib—a traveling salesman problem library. *ORSA Journal on Computing*, 3(4):376–384, 1991.

[30] Jimmy Lei Ba, Jamie Ryan Kiros, and Geoffrey E Hinton. Layer normalization. *arXiv preprint arXiv:1607.06450*, 2016.

[31] Kaiming He, Xiangyu Zhang, Shaoqing Ren, and Jian Sun. Deep residual learning for image recognition. In *Proceedings of the IEEE Conference on Computer Vision and Pattern Recognition*, pages 770–778, 2016.

[32] Liang Xin, Wen Song, Zhiguang Cao, and Jie Zhang. Step-wise deep learning models for solving routing problems. *IEEE Transactions on Industrial Informatics*, 17(7):4861–4871, 2020.

[33] Ronald J Williams. Simple statistical gradient-following algorithms for connectionist reinforcement learning. *Machine Learning*, 8:229–256, 1992.

[34] Qingchun Hou, Jingwei Yang, Yiqiang Su, Xiaoqing Wang, and Yuming Deng. Generalize learned heuristics to solve large-scale vehicle routing problems in real-time. In *The Eleventh International Conference on Learning Representations*, 2022.

[35] Florian Arnold, Michel Gendreau, and Kenneth Sørensen. Efficiently solving very large-scale routing problems. *Computers & operations research*, 107:32–42, 2019.

[36] Diederik P Kingma and Jimmy Ba. Adam: A method for stochastic optimization. *arXiv preprint arXiv:1412.6980*, 2014.

[37] David Applegate, Rober Bixby, Vasek Chvatal, and William Cook. Concorde tsp solver, 2006.

[38] Jianan Zhou, Yaxin Wu, Wen Song, Zhiguang Cao, and Jie Zhang. Towards omni-generalizable neural methods for vehicle routing problems. In *International Conference on Machine Learning*, 2023.

[39] Haoran Ye, Jiarui Wang, Helan Liang, Zhiguang Cao, Yong Li, and Fanzhang Li. Glop: Learning global partition and local construction for solving large-scale routing problems in real-time. In *Proceedings of the AAAI Conference on Artificial Intelligence*, volume 38, pages 20284–20292, 2024.

[40] Fu Luo, Xi Lin, Zhenkun Wang, Xialiang Tong, Mingxuan Yuan, and Qingfu Zhang. Self-improved learning for scalable neural combinatorial optimization. *arXiv preprint arXiv:2403.19561*, 2024.

[41] Paolo Toth and Daniele Vigo. *The vehicle routing problem*. SIAM, 2002.

[42] Mohammadreza Nazari, Afshin Oroojlooy, Lawrence Snyder, and Martin Takáć. Reinforcement learning for solving the vehicle routing problem. *Advances in Neural Information Processing Systems*, 31, 2018.

[43] Yubin Xiao, Di Wang, Boyang Li, Huanhuan Chen, Wei Pang, Xuan Wu, Hao Li, Dong Xu, Yanchun Liang, and You Zhou. Reinforcement learning-based nonautoregressive solver for traveling salesman problems. *IEEE Transactions on Neural Networks and Learning Systems*, 2024.

[44] Liang Xin, Wen Song, Zhiguang Cao, and Jie Zhang. Multi-decoder attention model with embedding glimpse for solving vehicle routing problems. In *Proceedings of the AAAI Conference on Artificial Intelligence*, volume 35, pages 12042–12049, 2021.

[45] André Hottung and Kevin Tierney. Neural large neighborhood search for the capacitated vehicle routing problem. In *European Conference on Artificial Intelligence*, 2020.

[46] Xinyun Chen and Yuandong Tian. Learning to perform local rewriting for combinatorial optimization. *Advances in Neural Information Processing Systems*, 32, 2019.

[47] Michel Deudon, Pierre Cournut, Alexandre Lacoste, Yossiri Adulyasak, and Louis-Martin Rousseau. Learning heuristics for the tsp by policy gradient. In *Integration of Constraint Programming, Artificial Intelligence, and Operations Research: 15th International Conference, CPAIOR 2018, Delft, The Netherlands, June 26–29, 2018, Proceedings 15*, pages 170–181. Springer, 2018.

[48] André Hottung, Yeong-Dae Kwon, and Kevin Tierney. Efficient active search for combinatorial optimization problems. In *International Conference on Learning Representations*, 2022.

[49] Minsu Kim, Jinkyoo Park, et al. Learning collaborative policies to solve np-hard routing problems. *Advances in Neural Information Processing Systems*, 34:10418–10430, 2021.

[50] Sirui Li, Zhongxia Yan, and Cathy Wu. Learning to delegate for large-scale vehicle routing. *Advances in Neural Information Processing Systems*, 34:26198–26211, 2021.

[51] Xuanhao Pan, Yan Jin, Yuandong Ding, Mingxiao Feng, Li Zhao, Lei Song, and Jiang Bian. H-tsp: Hierarchically solving the large-scale travelling salesman problem. In *Proceedings of the AAAI Conference on Artificial Intelligence*, 2023.

[52] Zhi Zheng, Changliang Zhou, Tong Xialiang, Mingxuan Yuan, and Zhenkun Wang. Udc: A unified neural divide-and-conquer framework for large-scale combinatorial optimization problems. In *Thirty-eighth Conference on Neural Information Processing Systems*, 2024.

[53] Cong Zhang, Wen Song, Zhiguang Cao, Jie Zhang, Puay Siew Tan, and Xu Chi. Learning to dispatch for job shop scheduling via deep reinforcement learning. *Advances in Neural Information Processing Systems*, 33:1621–1632, 2020.

[54] Cong Zhang, Zhiguang Cao, Wen Song, Yaxin Wu, and Jie Zhang. Deep reinforcement learning guided improvement heuristic for job shop scheduling. In *International Conference on Learning Representations*, 2024.

[55] Dinghuai Zhang, Hanjun Dai, Nikolay Malkin, Aaron C Courville, Yoshua Bengio, and Ling Pan. Let the flows tell: Solving graph combinatorial problems with gflownets. *Advances in neural information processing systems*, 36:11952–11969, 2023.

[56] Yang Li, Jinpei Guo, Runzhong Wang, Hongyan Zha, and Junchi Yan. Fast t2t: Optimization consistency speeds up diffusion-based training-to-testing solving for combinatorial optimization. *Advances in Neural Information Processing Systems*, 37:30179–30206, 2024.

[57] Zhihao Xing and Shikui Tu. A graph neural network assisted monte carlo tree search approach to traveling salesman problem. *IEEE Access*, 8:108418–108428, 2020.

[58] Yimeng Min, Yiwei Bai, and Carla P Gomes. Unsupervised learning for solving the travelling salesman problem. *Advances in Neural Information Processing Systems*, 36, 2023.

[59] Yifan Xia, Xianliang Yang, Zichuan Liu, Zhihao Liu, Lei Song, and Jiang Bian. Position: Rethinking post-hoc search-based neural approaches for solving large-scale traveling salesman problems. In *International Conference on Machine Learning*, pages 54178–54190. PMLR, 2024.

[60] Ashish Vaswani, Noam Shazeer, Niki Parmar, Jakob Uszkoreit, Llion Jones, Aidan N Gomez, Łukasz Kaiser, and Illia Polosukhin. Attention is all you need. *Advances in Neural Information Processing Systems*, 30, 2017.

A Definitions and Formulations of TSP and CVRP

In this section, we provide the definitions and mathematical formulations of the Traveling Salesman Problem (TSP) and the Capacitated Vehicle Routing Problem (CVRP), thereby enabling readers to obtain a clearer and more profound understanding of the fundamental nature of these problems.

A.1 Traveling Salesman Problem (TSP)

The TSP is one of the most representative combinatorial optimization problems, and we focus on the 2D Euclidean TSP in this paper [14, 16]. Given an instance $S = \{\mathbf{s}_i\}_{i=1}^n$ with node features $\mathbf{s}_i \in \mathbb{R}^2$, represented as a sequence of n cities in a two-dimensional space. We are concerned with finding a permutation of the nodes $\pi = (\pi_1, \pi_2, \pi_3, \dots, \pi_n)$, termed a tour, that visits each city once and has the minimum total length. We define the length of a tour defined by a permutation π as

$$\text{minimize} \quad L(\pi|S) = \|\mathbf{s}_{\pi_n} - \mathbf{s}_{\pi_1}\| + \sum_{i=1}^{n-1} \|\mathbf{s}_{\pi_i} - \mathbf{s}_{\pi_{i+1}}\|, \quad (15)$$

where $\|\cdot\|$ represents ℓ_2 norm.

A.2 Capacitated Vehicle Routing Problem (CVRP)

A general formulation for CVRP with maximum vehicle number constraints ϵ_m [41, 34] is introduced in this section. Specifically, given a complete graph $G = (\Omega, E)$, binary variables $z_{ij} \in \{0, 1\}$ are defined to represent whether a vehicle traverses arc (i, j) in the solution. c_i and δ_i denote the remaining vehicle capacity after visiting customer i and the demand of customer i , respectively. The maximum capacity of each vehicle is denoted as C , respectively. Given these variables, the formulation is given as follows.

$$\text{minimize} \quad \sum_{i \in \Omega, j \in \Omega, i \neq j} d_{ij} z_{ij} \quad (16)$$

$$\text{subject to} \quad \sum_{j \in \Omega, i \neq j} x_{ij} = 1, \quad \forall i \in \Omega \setminus \{0\} \quad (17)$$

$$\sum_{i \in \Omega, i \neq j} x_{ij} = 1, \quad \forall j \in \Omega \setminus \{0\} \quad (18)$$

$$c_j = \begin{cases} c_i - \delta_j, & \text{if } z_{ij} = 1, \quad \forall (i, j) \in \Omega \\ c_j, & \text{if } z_{ij} = 0, \quad \forall (i, j) \in \Omega \end{cases} \quad (19)$$

$$c_j - c_i \geq \delta_j - C(1 - z_{ij}), \quad \forall i, j \in \Omega \setminus \{0\}, i \neq j, d_i + d_j \leq C \quad (20)$$

$$0 \leq c_i \leq C - \delta_i, \quad i \in \Omega \setminus \{0\} \quad (21)$$

$$\sum_{j \in \Omega \setminus \{0\}} z_{j0} = \epsilon \quad (22)$$

$$\sum_{i \in \Omega \setminus \{0\}} z_{i0} = \epsilon \quad (23)$$

$$\epsilon \leq \epsilon_m \quad (24)$$

$$z_{ij} \in \{0, 1\}, \quad \forall i, j \in \Omega, i \neq j \quad (25)$$

where Equation (16) is objective function, d_{ij} is the Euclidean distance from customer i to customer j . Equation (17) and Equation (18) ensure that each customer is visited exactly once. Equation (19) is the updating process of remaining vehicle capacity and Equation (20)–Equation (21) define the capacity and connectivity constraints. Equation (22)–Equation (24) ensure that the number of vehicles departing from the depot equals the total number returning to the depot, i.e., each vehicle must start and terminate its route at the depot.

B Related Work

B.1 NCO without Search Space Reduction

Most neural combinatorial optimization (NCO) models are trained on small-scale instances (e.g., 100 nodes) without search space reduction and achieve strong performance on instances of similar size. However, their effectiveness significantly diminishes when applied to larger instances (e.g., those exceeding 1,000 nodes) [42, 43, 44, 45, 46]. Some approaches incorporate additional search procedures, such as 2-opt [47] and active search [14, 48], to address this limitation. While these techniques can improve solution quality, they are still computationally expensive for large-scale instances. Another line of research focuses on training NCO models directly on larger-scale instances (e.g., up to 500 nodes) to enhance generalization [27, 38, 17]. However, this approach incurs prohibitive computational costs due to the exponentially growing search space. Alternatively, some methods simplify large-scale VRPs through decomposition policies [49, 50, 34, 51, 52]. Although effective, these methods often overlook the dependency between decomposition policies and subsequent solvers, resulting in suboptimal solutions. Moreover, the reliance on expert-designed policies limits their practicality for real-world applications. In addition, recent learning-based advancements also show promising results for non-routing problems, such as Job Shop Scheduling Problems [53, 54] and other graph problems (e.g., Maximum Independent Set and Maximum Clique) [55]. These approaches have proven particularly effective in dynamic environments where traditional methods face challenges.

B.2 NCO with Static Search Space Reduction

To address the scalability challenges of NCO methods, static search space reduction (SSR) has been proposed as a computationally efficient approach. These methods perform one-time pruning at the beginning of the optimization process, significantly reducing the problem size. For example, Sun et al. [21] develop a static problem reduction technique to eliminate unpromising edges in large-scale TSP instances. Recently, heatmap-based approaches have gained popularity for solving large-scale TSPs, where models are trained to predict the probability of each edge belonging to the optimal solution. To handle large-scale instances, these methods often incorporate graph sparsification [23, 24, 25, 56] or pruning strategies [57, 22, 58] to reduce the search space. While static SSR is computationally efficient, it typically requires additional well-designed search procedures (e.g., Monte Carlo Tree Search for TSP) to achieve high-quality solutions, which might be more important for the optimization process [59].

B.3 NCO with Dynamic Search Space Reduction

Dynamic search space reduction (SSR) has also been explored as a promising approach to address the scalability challenges of NCO methods. These methods adaptively prune the search space to a small set of candidate nodes at each construction step, typically based on the distance to the last visited node. The final node selection can be guided by either the original policy augmented with auxiliary distance information [27] or a well-designed local policy [26]. Additionally, recent work by Fang et al. [28] and Drakulic et al. [10] directly selects the next node from the candidate set using NCO models. While dynamic SSR can more efficiently reduce the search space for constructive NCO, its reliance on distance-based node selection is inappropriate for large-scale instances, especially those from non-uniform distributions.

C Further Analysis of Distance-based Search Space Reduction

C.1 Impact on Optimality Gap

In this subsection, we provide detailed solution visualizations across TSPLIB instances of varying scales under different levels of search space reduction (k). As shown in Figure 5, this degradation is primarily attributed to the elimination of non-local node selections that are crucial for optimal routes, and the cumulative effect of over-pruning during the solution construction process leads to significant deviations from the optimal route in subsequent node selections, ultimately compromising the overall solution quality obtained by D-SSR.

C.2 Impacts on Constructive NCOs

In this subsection, regarding the impacts of distance-based search space reduction across diverse constructive NCO architectures, we conduct further experimental analyses, which mainly include: (1) the impact for constructive NCO methods with a heavy decoder, (2) the impact for constructive NCO methods with a heavy encoder, and (3) the impact for the retrained constructive NCO method.

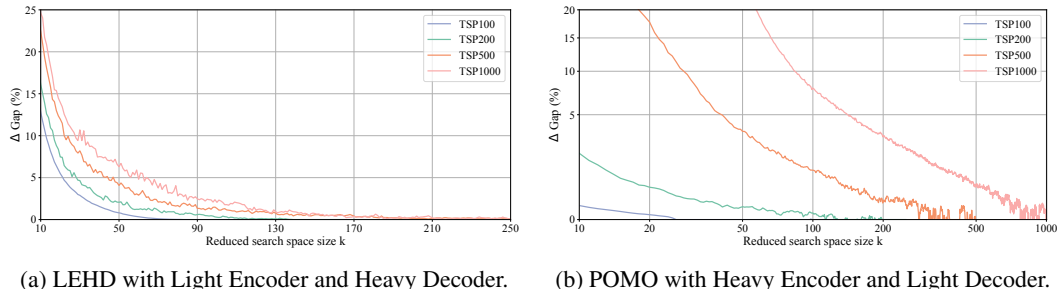


Figure 4: The effect of distance-based search space reduction on the gap in diverse constructive NCO architectures (Left: LEHD [9]; Right: POMO [18]). Here $\Delta\text{Gap} = \text{Gap}_{\text{reduced}} - \text{Gap}_{\text{original}}$.

C.2.1 Impact on Pretrained Constructive NCO

Impact on Constructive NCO with Heavy Decoder To evaluate the impact of search space reduction on NCO performance, we use the well-known LEHD method [9] as a representative example, restricting the search space to the k nearest nodes from the last visited node at each construction step. Without loss of generality, we use the LEHD-greedy without any RRC strategy. We quantify the impact by measuring the performance gap $\Delta\text{Gap} = \text{Gap}_{\text{reduced}} - \text{Gap}_{\text{original}}$, defined as the difference between the optimality gap obtained by LEHD with a reduced search space ($\text{Gap}_{\text{reduced}}$) and the original LEHD without search space reduction ($\text{Gap}_{\text{original}}$).

The results in Figure 4a illustrate the performance on TSP instances of varying sizes under different search space reduction levels (k). A key observation is the existence of a critical threshold k^* for each problem size, beyond which LEHD with $k \geq k^*$ achieves a 0% performance gap with the original LEHD, indicating no loss in solution quality with SSR. However, these critical thresholds vary significantly across problem sizes, and using a small $k < k^*$ leads to substantial performance degradation.

Impact on Constructive NCO with Heavy Encoder In addition to SL-based LEHD with a heavy decoder architecture, we also evaluate the RL-based POMO model featuring a heavy encoder architecture, and the instance augmentation technology is not used in our experiment. As shown in Figure 4b, our experimental results demonstrate a consistent phenomenon with the SL-based LEHD case: The critical thresholds k^* exhibit significant variations across different problem sizes, and using a small $k < k^*$ results in considerable performance deterioration.

C.2.2 Impact on Retrained Constructive NCO

Considering that the inconsistency between training and inference strategies may introduce a deviation between the model’s learned perception and its actual decision-making process, we retrain three

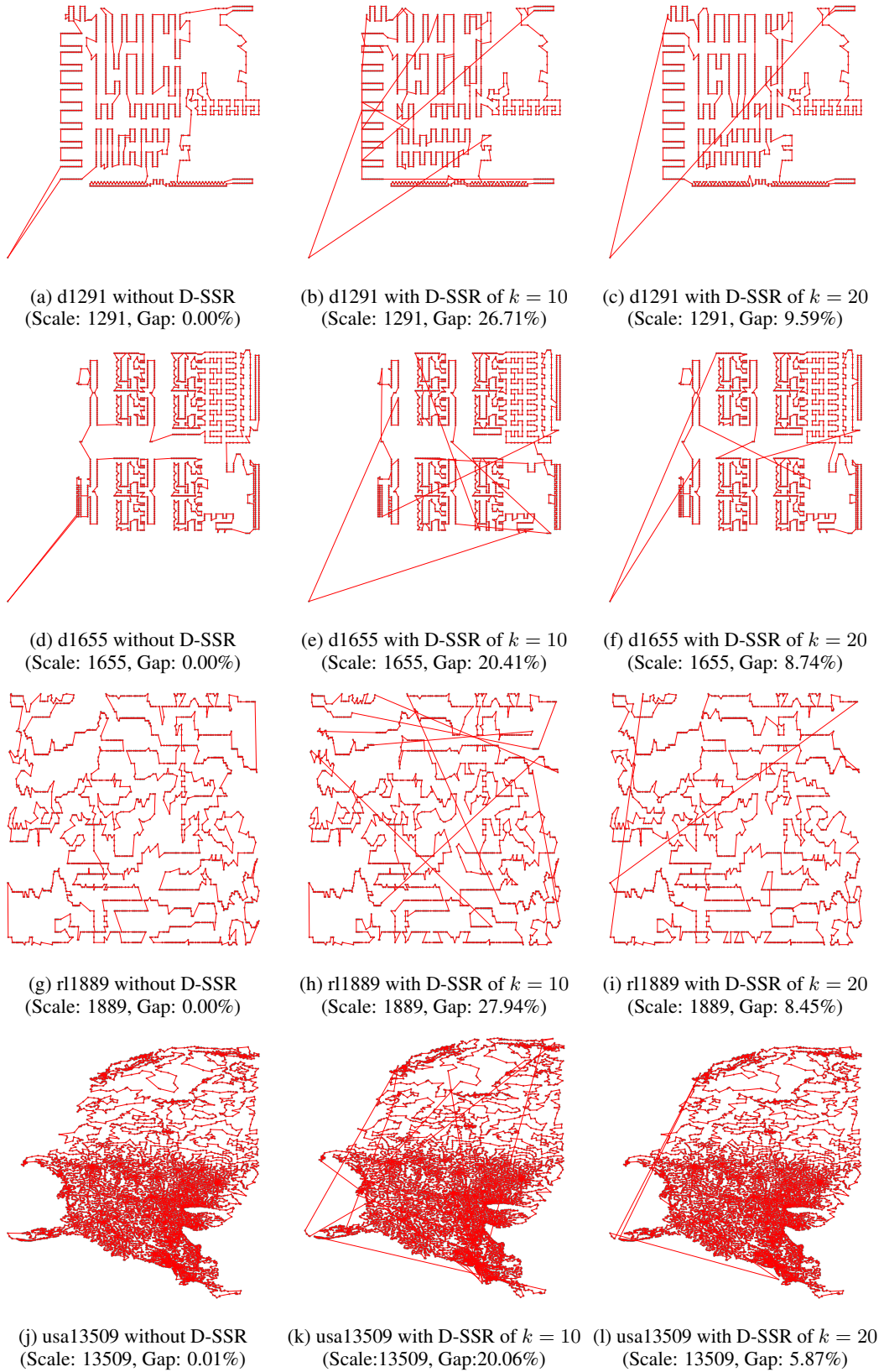


Figure 5: The solution visualizations of TSPLIB instances under different levels of search space. All solutions are obtained by the LKH-3 algorithm [3].

reduced variants of LEHD with different search space reduction configurations. As illustrated in Table 8, while reducing the search space significantly decreases inference time, employing an excessively small k based on pairwise distance information results in substantial performance deterioration.

Table 8: The effect of distance-based search space reduction on the gap in the LEHD model. Note that all LEHD models with search space reduction are retrained with the same specifications.

Method	TSP100		TSP200		TSP500		TSP1000	
	Gap	Time	Gap	Time	Gap	Time	Gap	Time
LKH3	0.00%	56m	0.00%	4m	0.00%	32m	0.00%	8.2h
LEHD w/ $k = 20$	3.10%	10.7s	5.21%	1.0s	7.95%	2.1s	11.09%	3.7s
LEHD w/ $k = 30$	1.71%	15s	3.03%	1.1s	6.01%	2.2s	9.44%	4s
LEHD w/ $k = 50$	0.87%	18.7s	1.74%	1.28s	4.03%	2.6s	7.41%	4.9s
LEHD w/o SSR	0.58%	24s	0.86%	3s	1.56%	18s	3.17%	1.6m

These findings highlight the potential of search space reduction while underscoring the need for advanced reduction methods capable of efficiently handling large-scale problems with a small k .

D Compatibility with Adaptation Bias

As defined in Equation (6), the adaptation bias between each feasible node $i \in \mathcal{A}_t$ and the current node π_{t-1} (selected by the local construction model) is given by $a_{t-1,i}^R = -\alpha \cdot \log_2 N \cdot d_{t-1,i}$, following Zhou et al. [17]. Here, N denotes the total number of nodes (i.e., problem size), and $\alpha > 0$ is a learnable parameter with a default value of 1 that enables the model to adaptively learn information-specific weights. This function incorporates both distance $d_{t-1,i}$ and scale information $\log_2 N$ to better capture varying geometric variations with different scales. Accurately identifying candidate nodes within a large search space remains challenging when relying solely on a lightweight network architecture. Unlike existing distance-based reduction methods, our approach addresses the trade-off between learning difficulty and solution quality by incorporating a distance-assisted reduction model to enhance neighborhood selection performance.

Additionally, we extend this adaptation bias to the compatibility computation in the local construction model. In Equation (10), the bias between each candidate node $i \in \mathcal{N}_t$ and the current node π_{t-1} is defined as $a_{t-1,i}^L = -\alpha \cdot \log_2 |\mathcal{N}_t| \cdot d_{t-1,i}$. Here, $|\mathcal{N}_t|$ denotes the total number of candidate nodes.

To evaluate the effectiveness of two adaptation biases, we conduct an ablation study with different component configurations, and the detailed results are provided in Appendix L.2.

E Learning-based Reduction Model for CVRPs

We develop a learning-based reduction model to dynamically evaluate the potential of feasible nodes and adaptively reduce the search space at each construction step. Our proposed model ensures efficiency through a lightweight architecture consisting of only an embedding layer and an attention layer. For CVRPs, we introduce a specialized treatment for each node to address the unique demands of the problem. In this section, we provide a detailed description of this specialized treatment for CVRPs in the reduction model.

Embedding Layer Given an instance $S = \{\mathbf{s}_i\}_{i=1}^{N+1}$ with node features $\mathbf{s}_i \in \mathbb{R}^{d_x}$ (i.e., node coordinates and demand), we feed depot and nodes into a unified linear layer. The detailed calculation is expressed as

$$\mathbf{h}_i^D = W^{(e)}[x_i, y_i, \delta_i] + \mathbf{b}^{(e)}, \quad i = 1, \dots, N+1, \quad (26)$$

where x_i and y_i denote the node coordinates, δ_i is the demand of node i , we regard the demand of depot as 0 (i.e., $\delta_0 = 0$), $W^{(e)} \in \mathbb{R}^{3 \times d}$ and $\mathbf{b}^{(e)} \in \mathbb{R}^d$ are learnable parameters. This process yields a set of embeddings $H^D = \{\mathbf{h}_i^D\}_{i=1}^{N+1}$ for all nodes in the instance S . At the t -th step, with a partial solution following Kwon et al. [18], we define a context embedding for the current partial solution:

$$\mathbf{h}_{(C_D)}^t = W_{\text{last}}[\mathbf{h}_{\pi_{t-1}}^D, Q_{\text{remain}}], \quad (27)$$

where $W_{\text{last}} \in \mathbb{R}^{(1+d) \times d}$ is a learnable matrix, and Q_{remain} represents the current remaining capacity.

Masking The static reduction stage performs partial search space reduction to obtain the pruned graph G' . In particular, we do not allow nodes to be visited if their remaining demand is either 0 (indicating the node has already been visited) or exceeds the remaining capacity of the vehicle. We denote \mathcal{A}_t as the set of all feasible nodes, and the embeddings of \mathcal{A}_t are represented by $H_{\mathcal{A}_t}^D = \{\mathbf{h}_i^D \mid i \in \mathcal{A}_t\} \in \mathbb{R}^{|\mathcal{A}_t| \times d}$.

F Local Solution Construction Model

The proposed local solution construction model includes four components: 1) coordinate normalization, 2) embedding layer, 3) attention layer, and 4) compatibility calculation, which are detailed in the following subsections.

F.1 Coordinate Normalization

We introduce a coordinate normalization operation to ensure that each extracted sub-graph G'_{sub} adheres to a similar distribution [22, 39, 28]. This operation not only simplifies the input feature space but also significantly enhances the stability and homogeneity of model inputs across different sub-graphs. Following Fu et al. [22] and Fang et al. [28], the coordinate transformation is formulated as

$$x^{\min} = \min_{i \in \mathcal{N}_t} x_i, \quad x^{\max} = \max_{i \in \mathcal{N}_t} x_i, \quad (28)$$

$$y^{\min} = \min_{i \in \mathcal{N}_t} y_i, \quad y^{\max} = \max_{i \in \mathcal{N}_t} y_i, \\ r = \frac{1}{\max(x^{\max} - x^{\min}, y^{\max} - y^{\min})}, \quad (29)$$

$$x_i^{\text{new}} = r \times (x_i - x^{\min}) \quad \forall i \in \{\pi_1, \pi_{t-1}\} \cup \mathcal{N}_t, \\ y_i^{\text{new}} = r \times (y_i - y^{\min}) \quad \forall i \in \{\pi_1, \pi_{t-1}\} \cup \mathcal{N}_t, \quad (30)$$

where x_i and y_i denote the node coordinates, and \mathcal{N}_t represents the k candidate nodes generated based on π_{t-1} and the dynamic reduction model. To ensure that the first visited node (or depot) π_1 remains within the boundary (i.e., $0 \leq x_i^{\text{new}} \leq 1$), we apply $x_i^{\text{new}} = \max(0, \min(x_i^{\text{new}}, 1))$, and the same operation is applied to y_i^{new} . Equations (28)–(30) effectively simplify the input feature space and improve the stability and homogeneity of model inputs across different sub-graphs. Subsequently, the sub-graph G'_{sub} is transformed into a new graph G''_{sub} .

F.2 Embedding Layer

Traveling Salesman Problem Given the converted sub-graph G''_{sub} , the embedding layer first transforms the coordinates into initial embeddings using a shared linear layer with learnable parameters $[W^{(0)} \in \mathbb{R}^{d_x \times d}; b^{(0)} \in \mathbb{R}^d]$. The embeddings of the k candidate nodes \mathcal{N}_t are denoted by $H_{\mathcal{N}}^{(0)} = \{\mathbf{h}_i^{(0)} \mid i \in \mathcal{N}_t\} \in \mathbb{R}^{k \times d}$. Here, the first node π_1 and the last node π_{t-1} are used to represent the current partial solution. Therefore, their initial embeddings require special treatment [10, 9]. Specifically, additional learnable matrices $W_1 \in \mathbb{R}^{d \times d}$ and $W_2 \in \mathbb{R}^{d \times d}$ are applied to $\mathbf{h}_{\pi_1}^{(0)}$ and $\mathbf{h}_{\pi_{t-1}}^{(0)}$, respectively. Accordingly, we define the initial graph node embeddings $\tilde{H}^{(0)} \in \mathbb{R}^{(2+|\mathcal{N}_t|) \times d}$ as

$$\tilde{H}^{(0)} = [W_1 \mathbf{h}_{\pi_1}^{(0)}, W_2 \mathbf{h}_{\pi_{t-1}}^{(0)}, H_{\mathcal{N}_t}^{(0)}], \quad (31)$$

where $[\cdot, \cdot]$ denotes the vertical concatenation operator. Next, $\tilde{H}^{(0)}$ is passed through the L attention layers sequentially.

Capacitated Vehicle Routing Problem For CVRP, due to the demands and capacity constraints, we introduce a specialized treatment for the initial embedding of each node. Specifically, the node demands are normalized as $\delta_i = \{\delta_i / Q_{\text{remain}} \mid i \in \mathcal{N}_t\}$, where Q_{remain} represents the remaining capacity. We separate the coordinates and demands and feed them into distinct linear layers. The detailed calculation is expressed as

$$\begin{aligned} \mathbf{h}_{i_{\text{coor}}}^{(0)} &= W^{(0)}[x_i, y_i] + \mathbf{b}^{(0)} \quad \forall i \in \{\pi_1, \pi_{t-1}\} \cup \mathcal{N}_t, \\ \mathbf{h}_i^{(0)} &= \mathbf{h}_{i_{\text{coor}}}^{(0)} + W_{\text{demand}} \delta_i \quad \forall i \in \mathcal{N}_t, \\ \mathbf{h}_{\pi_1}^{(0)} &= W_1 \mathbf{h}_{\pi_1_{\text{coor}}}^{(0)} + W_{\text{load}} Q_{\text{remain}}, \\ \mathbf{h}_{\pi_{t-1}}^{(0)} &= W_2 \mathbf{h}_{\pi_{t-1}_{\text{coor}}}^{(0)} + W_{\text{load}} Q_{\text{remain}}, \end{aligned} \quad (32)$$

where $W_{\text{demand}} \in \mathbb{R}^{1 \times d}$ and $W_{\text{load}} \in \mathbb{R}^{1 \times d}$ are learnable matrices used for demand and remaining capacity, respectively.

F.3 Attention Layer

Inspired by BQ [10] and LEHD [9], our attention layer consists of two sub-layers: an attention sub-layer and a feed-forward (FF) sub-layer. Both sub-layers incorporate Layer Normalization [30] and skip connections [31].

Let $\tilde{H}^{(\ell-1)} = [\mathbf{h}_{\pi_1}^{(\ell-1)}, \mathbf{h}_{\pi_{t-1}}^{(\ell-1)}, H_{\mathcal{N}_t}^{(\ell-1)}]$ denote the input to the ℓ -th attention layer for $\ell = 1, \dots, M$. The outputs for the i -th node are computed as follows:

$$\hat{\mathbf{h}}_i^{(\ell)} = \text{LN}^{(\ell)} \left(\mathbf{h}_i^{(\ell-1)} + \text{Attention}^{(\ell)} \left(\mathbf{h}_i^{(\ell-1)}, \tilde{H}^{(\ell-1)} \right) \right), \quad (33)$$

$$\mathbf{h}_i^{(\ell)} = \text{LN}^{(\ell)} \left(\hat{\mathbf{h}}_i^{(\ell)} + \text{FF}^{(\ell)} \left(\hat{\mathbf{h}}_i^{(\ell)} \right) \right), \quad (34)$$

where $\text{LN}(\cdot)$ denotes layer normalization [30], which mitigates potential value overflows caused by exponential operations; Attention in Equation (33) represents the adopted attention mechanism (see Appendix G for details), and $\text{FF}(\cdot)$ in Equation (34) corresponds to a fully connected neural network with ReLU activation.

After M attention layers, the final node embeddings $\tilde{H}^{(M)} = [\mathbf{h}_{\pi_1}^{(M)}, \mathbf{h}_{\pi_{t-1}}^{(M)}, H_{\mathcal{N}_t}^{(M)}] \in \mathbb{R}^{(2+|\mathcal{N}_t|) \times d}$ encapsulate the advanced feature representations of the first node, last node, and k candidate nodes.

F.4 Padding

To address the variability in the number of candidate nodes when solving a batch of instances, we pad the number of candidate nodes $|\mathcal{N}_t|$ to the maximum length by adding an all-zero tensor. The maximum length is computed as $\max\{\min\{k, |\mathcal{A}_{i,t}|\} \mid i \in \{1, \dots, B\}\}$, where k is the predefined search space size, $|\mathcal{A}_{i,t}|$ denotes the number of feasible unvisited nodes at the current step t for instance S_i , and B represents the batch size. An attention mask is then applied to mask out the padded zeros during computation.

G Adaptation Attention Free Module

Following Zhou et al. [17], we implement $\text{Attention}(\cdot)$ using a scale-distance adopted adaptation attention free module (AAFM) to enhance geometric pattern recognition for routing problems. Given the input X , AAFM first transforms it into Q , K , and V through corresponding linear projection operations:

$$Q = XW^Q, \quad K = XW^K, \quad V = XW^V, \quad (35)$$

where W^Q , W^K , and W^V are learnable matrices. The AAFM computation is then expressed as:

$$\text{Attention}(Q, K, V, A) = \sigma(Q) \odot \frac{\exp(A)(\exp(K) \odot V)}{\exp(A) \exp(K)}, \quad (36)$$

where σ denotes the sigmoid function, \odot represents the element-wise product, and $A = \{a_{ij}\}$ denotes the pair-wise adaptation bias. For more details about a_{ij} , please see Appendix D.

Compared to multi-head attention (MHA) [60], AAFM enables the model to explicitly capture instance-specific knowledge by updating pair-wise adaptation biases while exhibiting lower computational overhead. Further details are provided in the related work section mentioned above. For a detailed discussion of the comparison of AAFM and MHA in the L2R framework, please refer to Appendix L.3.

H Pseudocode for Training

Following Kool et al. [16], we employ an exponential baseline ($\beta = 0.8$) during the first epoch to stabilize initial learning. The baseline parameters θ^{BL} are updated only if the improvement is statistically significant, as determined by a paired t-test ($\alpha = 5\%$) conducted on 10,000 separate evaluation instances at the end of each epoch. If the baseline policy is updated, new evaluation instances are sampled to prevent overfitting. Additionally, at the first construction step for TSP, π_1 is randomly selected as the initial partial solution and is treated as both the initial and last nodes for the first decoding steps.

Algorithm 1 L2R Training with REINFORCE Algorithm

```

1: Input: number of epochs  $E$ , steps per epoch  $T$ , batch size  $B$ , significance  $\alpha$ , the percentage  $\gamma$  of
   static reduction.
2: Output: The trained model with parameters  $\theta = \{\theta_R, \theta_L\}$ , which are reduction model  $\theta_R$  and
   local construction model  $\theta_L$ .
3: Init  $\theta_R$ ,  $\theta_R^{BL} \leftarrow \theta_R$  and  $\theta_L$ ,  $\theta_L^{BL} \leftarrow \theta_L$ .
4: for epoch = 1, ...,  $E$  do
5:   for step = 1, ...,  $T$  do
6:      $G_i \leftarrow \text{RandomInstance}()$   $\forall i \in \{1, \dots, B\}$ 
7:      $G'_i \leftarrow \text{StaticReduction}(\gamma)$   $\forall i \in \{1, \dots, B\}$ 
8:     // For  $\theta$ , we use a decoding strategy of sampling according to the output probabilities.
9:     while not done do
10:    //  $\mathcal{N}_{i,t}$  denotes the  $k$  high-potential candidate nodes at step  $t$  given sparse graph  $G'_i$ 
        generated by  $\theta_R$ .
11:    // This selection  $\tau_{i,t}$  is only used for the loss calculation of the reduction model.
12:     $\mathcal{N}_{i,t}, \tau_{i,t} \leftarrow \text{DynamicReduction}(G'_i, \pi_{t-1}, \theta_R)$   $\forall i \in \{1, \dots, B\}$ 
13:    // This selection  $\pi_{i,t}$  generated by  $\theta_L$  is used as the node selection for the current step  $t$ .
14:     $\pi_{i,t} \leftarrow \text{LocalConstruction}(\pi_1, \pi_{t-1}, \mathcal{N}_{i,t}, \theta_L)$   $\forall i \in \{1, \dots, B\}$ 
15:  end while
16:  // For  $\theta^{BL}$ , we use a greedy decoding strategy according to the output probabilities.
17:  while not done do
18:     $\mathcal{N}_{i,t}^{BL} \leftarrow \text{DynamicReduction}(G'_i, \pi_{t-1}^{BL}, \theta_R^{BL})$   $\forall i \in \{1, \dots, B\}$ 
19:    // For  $\theta^{BL}$ , we only obtain the current node selection  $\pi_{i,t}^{BL}$  of  $\theta_L^{BL}$  for calculating the
        reward.
20:     $\pi_{i,t}^{BL} \leftarrow \text{LocalConstruction}(\pi_1^{BL}, \pi_{t-1}^{BL}, \mathcal{N}_{i,t}^{BL}, \theta_L^{BL})$   $\forall i \in \{1, \dots, B\}$ 
21:  end while
22:   $\nabla_{\theta_R} \mathcal{L}_R(\theta_R) \leftarrow \frac{1}{B} \sum_{i=1}^B (\mathcal{R}(\pi_i) - \mathcal{R}(\pi_i^{BL})) \nabla_{\theta_R} \log o(\tau_i)$ 
23:   $\nabla_{\theta_L} \mathcal{L}_L(\theta_L) \leftarrow \frac{1}{B} \sum_{i=1}^B (\mathcal{R}(\pi_i) - \mathcal{R}(\pi_i^{BL})) \nabla_{\theta_L} \log p(\pi_i)$ 
24:   $\mathcal{L}_{\text{Joint}}(\theta) \leftarrow \mathcal{L}_R(\theta_R) + \mathcal{L}_L(\theta_L)$ 
25:   $\theta \leftarrow \text{Adam}(\theta, \nabla \mathcal{L}_{\text{Joint}})$ 
26: end for
27: if OneSidedPairedTTest( $p_{\theta}$ ,  $p_{\theta^{BL}}$ ) <  $\alpha$  then
28:    $\theta_R^{BL} \leftarrow \theta_R$ 
29:    $\theta_L^{BL} \leftarrow \theta_L$ 
30: end if
31: end for

```

I Training and Model Settings

Here, we provide the hyperparameter settings for the model and training process, and the detailed information can be found in Table 9.

Table 9: Training settings in our experiments.

Hyperparameter	TSP	CVRP
Optimizer	Adam	
Initial learning rate of θ_R	10^{-4}	
Learning rate decay of θ_R	0.98 per epoch	
Initial learning rate of θ_L	10^{-4}	
Learning rate decay of θ_L	0.98 per epoch	
Batch size	180	60
Batches of each epoch		2,500
Training scale		100
Epochs		100
The number of attention layer of θ_L	6	
Embedding dimension	128	
Feed forward dimension	512	
Clipping parameter ξ	10	
Training capacity	—	50
Maximum search space size k	20	50
Percentage γ of static reduction		10%
Gradient clipping		max_norm=1.0
Training baseline (epoch = 1)		Exponential baseline ($\beta = 0.8$)
Training baseline (epoch > 1)		Greedy rollout baseline

J Case-by-case Results on Benchmark Datasets

J.1 L2R vs. Algorithmic Methods

Taking the TSPLIB dataset as an example, we add the results of algorithmic methods (i.e., LKH3 and Concorde). As shown in Table 10, LKH3 and Concorde can outperform L2R on large-scale real-world instances, but they require a much longer runtime to obtain high-quality solutions. In addition, it should be emphasized that L2R can outperform all the other NCO methods with fast runtime on all comparisons, detailed results are provided in Table 11.

Table 10: Comparison between L2R and algorithmic methods (i.e., LKH-3 and Concorde) on large-scale TSPLIB instances ($5,000 \leq N \leq 85,900$). Here, "BKS" denotes the best-known solution.

Instance	Scale	BKS	LKH-3		Concorde		L2R		L2R PRC100	
			Gap	Time	Gap	Time	Gap	Time	Gap	Time
rl5915	5,915	565,530	0.00%	1.2h	0.29%	1.1h	10.04%	29s	6.37%	4.6m
rl5934	5,934	556,045	0.00%	1.3h	0.23%	1.2h	12.39%	29s	7.20%	5.2m
pla7397	7,397	23,260,728	0.00%	11.8h	0.22%	1.0h	7.22 %	36s	3.25%	5.2m
rl11849	11,849	923,288	0.00%	4.8h	0.66%	1.1h	6.96%	58s	4.49%	5.4m
usa13509	13,509	19,982,859	0.00%	7.5h	0.25%	1.2h	6.99%	1.1m	4.89%	5.4m
brd14051	14,051	469,385	0.00%	9.1h	0.39%	1.1h	6.52%	1.1m	4.16%	5.5m
d15112	15,112	1,573,084	0.00%	11.4h	0.26%	1.1h	7.55 %	1.2m	5.35%	5.2m
d18512	18,512	645,238	0.00%	13.1h	0.39%	1.1h	5.39%	1.5m	3.37%	5.8m
pla33810	33,810	66,048,945	0.00%	18h		N/A	6.37%	2.8m	4.35%	7.4m
pla85900	85,900	142,382,641	0.00%	23h		N/A	4.21%	7.7m	2.32%	12.9m
Avg.gap & Time			0.00%	10.1h	0.34%†	1.1h	7.36%	1.8m	4.58%	6.3m

† The pla33810 and pla85900 instances are skipped due to infeasible solution generation.

J.2 L2R vs. Classical Neural Solvers

We evaluate the generalization performance on instances from CVRPLIB Set-XXL [35] and TSPLIB [29]. Detailed results for large-scale instances are provided in Table 11. The results demonstrate that L2R consistently outperforms other models across instances of varying scales, demonstrating its strong applicability in real-world scenarios.

Table 11: The detailed results on large-scale TSPLIB [29] instances ($5,000 \leq N \leq 85,900$) and CVRPLIB [35] instances ($3,000 \leq N \leq 30,000$).

Instance	Scale	GLOP	BQ bs16	LEHD greedy	LEHD RRC1000	POMO aug $\times 8$	ELG aug $\times 8$	INViT greedy	L2R greedy	L2R PRC100
rl5915	5,915	11.56%	19.58%	24.17%	12.38%	OOM	OOM	14.02%	10.04%	6.37%
rl5934	5,934	11.32%	24.53%	24.11%	11.94%	OOM	OOM	12.91%	12.39%	7.20%
pla7397	7,397	6.38%	47.63%	40.94%	15.31%	OOM	OOM	9.45%	7.22%	3.25%
rl11849	11,849	9.55%	OOM	38.04%	18.19%	OOM	OOM	12.71%	6.96%	4.49%
usa13509	13,509	5.81%	OOM	71.10%	31.37%	OOM	OOM	13.44%	6.99%	4.89%
brd14051	14,051	4.87%	OOM	41.22%	21.19%	OOM	OOM	9.31%	6.52%	4.16%
d15112	15,112	4.90%	OOM	35.82%	18.83%	OOM	OOM	7.58%	7.55%	5.35%
d18512	18,512	4.99%	OOM	OOM	OOM	OOM	OOM	6.62%	5.39%	3.37%
pla33810	33,810	9.53%	OOM	OOM	OOM	OOM	OOM	7.04%	6.37%	4.35%
pla85900	85,900	7.97%	OOM	OOM	OOM	OOM	OOM	7.21%	4.21%	2.32%
Solved#		10/10	3/10	7/10	7/10	0/10	0/10	10/10	10/10	10/10
Avg.gap		7.69%	30.58% \dagger	39.34% \dagger	18.46% \dagger	—	—	10.03%	7.36%	4.58%
Instance	Scale	GLOP- LKH3	BQ bs16	LEHD greedy	LEHD RRC1000	POMO aug $\times 8$	ELG aug $\times 8$	INViT greedy	L2R greedy	L2R PRC100
Leuven1	3,000	14.95%	15.39%	16.60%	10.71%	460.32%	12.12%	13.71%	11.49%	5.67%
Leuven2	4,000	16.54%	25.69%	34.85%	21.22%	202.17%	21.52%	26.08%	12.73%	11.82%
Antwerp1	6,000	19.08%	13.64%	14.66%	8.91%	OOM	OOM	15.40%	11.04%	5.93%
Antwerp2	7,000	17.72%	26.09%	22.77%	15.42%	OOM	OOM	27.75%	12.95%	11.07%
Ghent1	10,000	18.28%	OOM	27.23%	17.28%	OOM	OOM	15.87%	10.15%	6.02%
Ghent2	11,000	16.45%	OOM	38.36%	25.77%	OOM	OOM	30.78%	11.29%	11.01%
Brussels1	15,000	26.17%	OOM	OOM	OOM	OOM	OOM	18.09%	12.65%	8.03%
Brussels2	16,000	17.56%	OOM	OOM	OOM	OOM	OOM	32.08%	12.30%	11.79%
Flanders1	20,000	24.02%	OOM	OOM	OOM	OOM	OOM	23.41%	7.85%	6.48%
Flanders2	30,000	25.42%	OOM	OOM	OOM	OOM	OOM	39.60%	13.09%	12.70%
Solved#		10/10	4/10	6/10	6/10	2/10	2/10	10/10	10/10	10/10
Avg.gap		19.62%	20.20% \dagger	25.75% \dagger	16.55% \dagger	331.24% \dagger	16.82% \dagger	24.28%	11.55%	9.34%

\dagger Some instances are skipped due to the OOM issue.

K Additional Analyses

K.1 L2R vs. D-SSR

To validate the effectiveness of our proposed L2R, we conduct a comparative experiment against a dynamic distance-based SSR model (i.e., D-SSR), ensuring identical experimental settings. We systematically analyze the advantages of L2R, mainly including: (1) overall performance on real-world instances, (2) optimality gap and optimality ratio per instance, (3) impacts of different candidate node selection strategies, and (4) solution visualizations comparing the two approaches.

K.1.1 Overall Performance on Real-world Instances

According to the results in Table 12, compared with traditional D-SSR, our proposed L2R can obtain better generalization performance in large-scale TSPLIB and CVRPLIB instances. Notably, this advantage becomes more pronounced when solving complex CVRP instances, where L2R significantly improves the final solution quality compared with D-SSR.

Table 12: Optimality gap comparison between two different candidate node selection approaches. Here, D-SSR denotes distance-based search space reduction.

Method	TSPLIB			CVRPLIB-XXL		
	$1K \leq N \leq 5K$ (23 instances)	$5K < N \leq 100K$ (10 instances)	All (33 instances)	$3K \leq N \leq 7K$ (4 instances)	$7K < N \leq 30K$ (6 instances)	All (10 instances)
D-SSR greedy	9.65%	7.47%	8.98%	14.38%	12.19%	13.06%
L2R greedy	9.16%	7.36%	8.61%	12.05%	11.22%	11.55%

K.1.2 Optimality Gap vs. Optimality Ratio

We then measure the optimality gap and optimality ratio per instance. The optimality ratio is defined as the proportion of nodes where the optimal next-visit node is located within the k candidate nodes of the current node. As demonstrated in Table 13, L2R achieves superior solution quality over D-SSR on real-world datasets. Although L2R exhibits only marginal improvement in the optimality ratio of next-visit node selection, the cumulative effect of over-pruning during the solution construction process leads to significant deviations from the optimal route in subsequent node selections, ultimately compromising the overall solution quality obtained by D-SSR.

K.1.3 Impacts of Candidate Node Selection Strategy

Figure 6 presents further analysis of candidate node selection across different reduction approaches at identical construction steps. The results in Figure 6a–Figure 6b indicate that while both D-SSR and L2R models successfully include the majority of optimal nodes within their generated neighborhoods, D-SSR exhibits significantly degraded solution quality. This degradation can be primarily attributed to its failure to include a critical minority of nodes within its candidate set. Consequently, the local construction model struggles in effectively selecting the optimal next-visit node. These critical nodes are exemplified by those to lead the sub-problem into a suboptimal state (see Figure 6c–Figure 6d) or manifest as anomalous single-node visits (see Figure 6e–Figure 6f). In contrast, the enhanced candidate selection capability of L2R allows it to capture more accurate candidate nodes, which facilitates better sequential decision-making and ultimately yields superior overall performance.

K.1.4 Solution Visualizations

To further support our argument, we provide additional solution visualizations comparing L2R and D-SSR. As illustrated in Figure 7, L2R tends to follow the optimal route more closely, but the cumulative effect of over-pruning during the solution construction of D-SSR leads to significant deviations in subsequent node selections. These deviations are a direct consequence of critical nodes not being adequately included in the candidate set, ultimately resulting in a significant degradation of D-SSR’s solution quality compared to L2R.

Table 13: Comparison of different reduction approaches on TSPLIB and CVRPLIB instances. All results are obtained with greedy decoding. "#Accuracy" measures the number of construction steps where the optimal next-visit node is contained within the top- k candidates selected by either learning-based or distance-based reduction methods. "Optimality Ratio" measures the proportion of nodes where the optimal next-visit node is located within the k candidate nodes of the current node. (i.e., $\#Accuracy * 100\% / N$).

	Instance	Scale	Gap ↓			#Accuracy (Optimality Ratio) ↑		
			D-SSR	L2R	ΔGap ↓	D-SSR	L2R	Δ#Accuracy ↑
TSPLIB	pcb1173	1173	5.17%	4.02%	-1.15%	1062 (90.54%)	1067 (90.96%)	+5
	rl1304	1304	9.88%	8.14%	-1.74%	1225 (93.94%)	1234 (94.63%)	+9
	rl1323	1323	16.44%	9.34%	-7.10%	1242 (93.88%)	1252 (94.63%)	+10
	u1817	1817	17.60%	9.54%	-8.06%	1614 (88.83%)	1630 (89.71%)	+16
	d2103	2103	20.50%	8.09%	-12.41%	1988 (94.53%)	2000 (95.10%)	+12
	pr2392	2392	10.72%	8.08%	-2.64%	2105 (88.00%)	2129 (89.01%)	+24
	fnl4461	4461	6.85%	4.22%	-2.63%	3871 (86.77%)	3896 (87.34%)	+25
	rl11849	11849	8.13%	6.96%	-1.17%	10851 (91.58%)	10864 (91.69%)	+13
	usa13509	13509	8.97%	6.99%	-1.98%	11886 (87.99%)	11947 (88.44%)	+61
CVRPLIB	pla33810	33810	7.57%	6.37%	-1.20%	30263 (89.51%)	30463 (90.10%)	+200
	Leuven1	3000	12.67%	11.49%	-1.18%	2284 (76.13%)	2294 (76.47%)	+10
	Leuven2	4000	15.71%	12.73%	-2.98%	3287 (82.18%)	3299 (82.48%)	+12
	Antwerp1	6000	13.12%	11.04%	-2.08%	4573 (76.22%)	4597 (76.62%)	+24
	Antwerp2	7000	16.00%	12.95%	-3.05%	5611 (80.16%)	5638 (80.54%)	+27
	Ghent1	10000	11.68%	10.15%	-1.53%	7658 (76.58%)	7665 (76.65%)	+7
	Ghent2	11000	13.55%	11.29%	-2.26%	9024 (82.04%)	9045 (82.23%)	+21
	Brussels2	16000	13.83%	12.30%	-1.53%	13099 (81.87%)	13109 (81.93%)	+10

K.2 Complexity Analysis

We present the time and space complexity of three different constructive models: L2R with learning-based SSR, INVIT with distance-based SSR, and LEHD without SSR. For the L2R method, we decompose the computational complexity into three key components: (1) the complexity of search space reduction (denoted as STEP1), (2) the complexity of local solution construction (denoted as STEP2), and (3) the overall framework complexity.

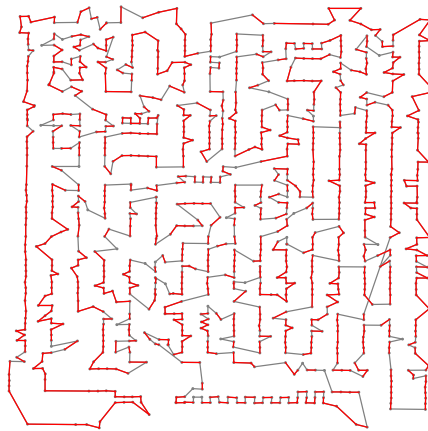
Table 14: Complexity analysis between L2R and existing works. Note that N and k denote the scale and the number of local neighbors, respectively. All results are obtained using greedy decoding. "Time" denotes the total inference time in the construction process, and "#m" is the number of tested instances.

Method	Time Complexity	Space Complexity	TSP5K(#16)		TSP10K(#16)		CVRP5K(#100)		CVRP10K(#16)	
			Gap	Time	Gap	Time	Gap	Time	Gap	Time
LEHD	$\mathcal{O}(N^3)$	$\mathcal{O}(N^2)$	15.46%	24m	27.24%	3.1h	9.51%	2.3h	13.25%	3.2h
INVIT-3V†	$\mathcal{O}(N(k_1^2 + k_2^2 + k_3^2 + k_1))$	$\mathcal{O}(k_1^2 + k_2^2 + k_3^2 + k_1)$	6.84%	3.4m	7.09%	9.3m	15.87%	11.6m	15.53%	19.2m
L2R-STEP1‡	$\mathcal{O}(N^2)$	$\mathcal{O}(N)$	—	8.0s	—	21.4s	—	17.5s	—	18.1s
L2R-STEP2‡	$\mathcal{O}(Nk^2)$	$\mathcal{O}(k^2)$	—	21.5s	—	42.6s	—	34.1s	—	52.1s
L2R	$\mathcal{O}(N^2 + Nk^2)$	$\mathcal{O}(N + k^2)$	4.69%	29.5s	4.82%	1.1m	7.74%	51.6s	4.18%	1.2m

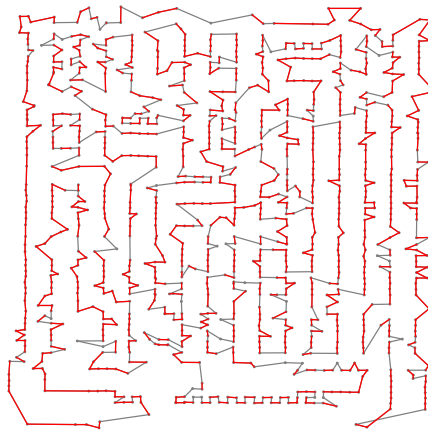
† For INVIT, k_1, k_2, k_3 represent different view, respectively.

‡ L2R-STEP1 and L2R-STEP2 represent the learning-based reduction model and local solution construction model, respectively.

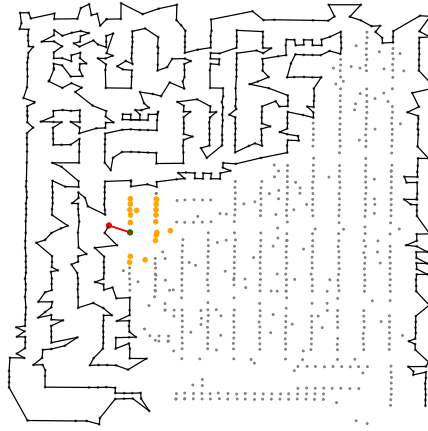
Our comparative results in Table 14 demonstrate that L2R-STEP2 achieves significantly lower computational complexity than both LEHD and INVIT. This efficiency advantage translates into substantially reduced runtime compared to existing representative models. Since distance-based SSR may compromise solution optimality, we introduce a learning-based reduction model to refine candidate node selection, thereby mitigating its negative impact. Although the reduction model incurs linear time complexity growth with problem size, experimental results demonstrate that the additional computational cost is justified, and L2R can perform better than D-SSR in solution quality. For more results and analyses, please see Appendix K.1.



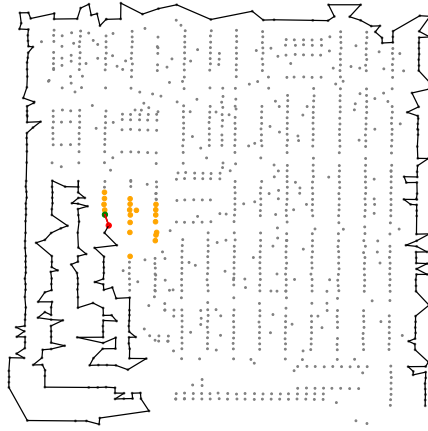
(a) D-SSR (Gap:5.17%, #Optimal: 906)



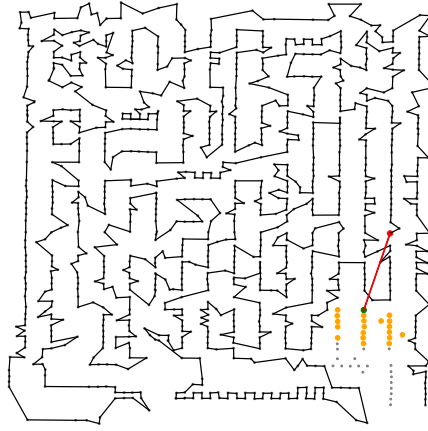
(b) L2R (Gap:4.02%, #Optimal: 928)



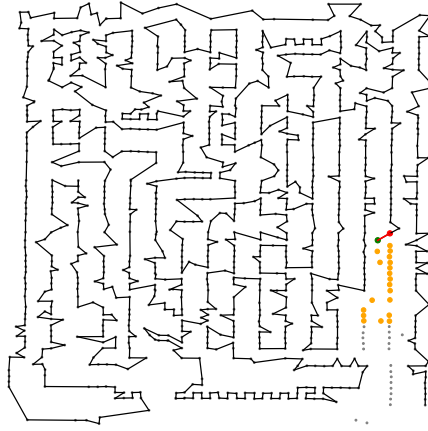
(c) Partial solution and candidate nodes (D-SSR)



(d) Partial solution and candidate nodes (L2R)



(e) Partial solution and candidate nodes (D-SSR)



(f) Partial solution and candidate nodes (L2R)

Figure 6: **The distributions of node selection strategy between different node selection approaches in TSPLIB, using pcb1173 as an example.** The solutions are all generated by greedy decoding. In (a)-(b), the red connections and "#Optimal" indicate optimal node connections and the number of optimal connections, respectively. For the remaining figures, the red, green, and orange nodes indicate the current node, the next visiting node, and candidate nodes, respectively.



Figure 7: **The solution visualizations of TSPLIB instances with different scales.** The solutions are all generated by greedy decoding. "Ratio" represents the optimality ratio, i.e., the proportion of nodes where the optimal next-visit node is located within the candidate nodes of the current node.

L Ablation Study

In this section, we conduct a detailed ablation study and analysis to demonstrate the effectiveness and robustness of L2R. Please note that, unless stated otherwise, the results presented in the ablation study are obtained with greedy decoding, and the performance of TSP instances is used as the primary criterion for evaluation.

L.1 L2R vs. Distance-based SSR with Larger Search Space

We conduct comparative experiments between four D-SSR models with varying search space sizes ($k \in \{20, 50, 75, 100\}$) and our proposed L2R model ($k = 20$) on TSP100K instances. We report the results obtained from greedy decoding and a PRC improvement procedure with different iterations.

Table 15: Comparison between learning-based small space and distance-based large space on TSP100K instances with uniform distribution.

Method	Greedy	PRC100	PRC500	PRC1000
D-SSR ($k = 20$)	5.09%	4.02%	3.49%	3.26%
D-SSR ($k = 50$)	6.62%	4.98%	4.23%	3.92%
D-SSR ($k = 75$)	7.33%	5.05%	4.20%	3.87%
D-SSR ($k = 100$)	5.74%	4.91%	4.20%	3.87%
L2R ($k = 20$)	4.79%	3.70%	3.21%	3.00%

The results in Table 15 show that our L2R model consistently achieves superior performance compared to distance-based SSR models, despite operating with a significantly smaller search space (L2R with $k = 20$ vs. D-SSR with $k \geq 20$). Furthermore, when combined with PRC, L2R also maintains this performance advantage over all D-SSR variants.

L.2 Effects of Adaptation Bias in Compatibility

Table 16: Comparison between different component settings of the compatibility module. Here, $a_{t-1,i}^R$ and $a_{t-1,i}^L$ indicate the adaptation bias adopted in Equation (6) and Equation (10), respectively.

$a_{t-1,i}^R$	$a_{t-1,i}^L$	TSP1K	TSP5K	TSP10K	TSP50K	TSP100K
×	×	53.91%	120.91%	157.46%	255.16%	305.95%
×	✓	56.64%	129.57%	169.68%	279.63%	335.51%
✓	×	5.22%	5.42%	5.66%	5.72%	5.68%
✓	✓	4.49%	4.69%	4.82%	4.86%	4.79%

To evaluate the effectiveness of two adaptation biases, we conduct an ablation study with different component configurations. The results in Table 16 demonstrate that accurately identifying candidate nodes within a large search space remains challenging when relying solely on a lightweight network architecture. Unlike existing distance-based reduction methods, our approach addresses the trade-off between learning difficulty and solution quality by incorporating a distance-assisted reduction model to enhance neighborhood selection performance. Both $a_{t-1,i}^R$ and $a_{t-1,i}^L$ contribute significantly to the promising model performance.

L.3 Comparison between Different Attention Mechanisms

Following Zhou et al. [17], we employ AAFM to implement $\text{Attention}(\cdot)$, enhancing geometric pattern recognition for routing problems (see Appendix G for implementation details). To evaluate the effectiveness of AAFM compared to the standard MHA in search space reduction and local construction, we train a variant of our L2R, denoted as L2R-MHA, which replaces AAFM with MHA. Furthermore, we introduce an adaptation version of L2R-MHA, termed L2R-MHA*, which incorporates an adaptation bias. Due to the special design of MHA, the integration of the adaptation

bias with self-attention is formulated as follows:

$$\text{Attention}^*(Q, K, V, A) = \text{softmax} \left(\frac{QK^T}{\sqrt{d_k}} + A \right) V, \quad (37)$$

where $A = \{\mathbf{a}_{ij}\}$ denotes the pair-wise adaptation bias computed by our adaptation function $f(N, d_{ij})$ in Appendix D. L2R-MHA and L2R-MHA* are trained in exactly the same training settings. The only difference between the three models is the attention mechanism.

Table 17: Comparison of different attention mechanisms on TSP instances with different scales. Here, "Time" denotes the total inference time.

Method	TSP1K		TSP5K		TSP10K		TSP50K		TSP100K	
	Gap	Time	Gap	Time	Gap	Time	Gap	Time	Gap	Time
L2R-MHA	6.90%	6.7s	7.36%	29.6s	7.54%	1.1m	7.79%	9.6m	7.72%	31.7m
L2R-MHA*	5.36%	7.0s	5.57%	31.0s	5.83%	1.1m	5.92%	9.8m	6.23%	32.2m
L2R	4.49%	6.5s	4.69%	29.5s	4.82%	1.1m	4.86%	9.5m	4.79%	29.4m

As shown in Table 17, the L2R-MHA and L2R-MHA* models demonstrate robust large-scale generalization capabilities, further validating the effectiveness of the proposed L2R framework. Notably, substituting the MHA mechanism with AAFM yields additional performance improvements with shorter runtime.

M Licenses for Used Resources

Table 18: List of licenses for the codes and datasets we used in this work

Resource	Type	Link	License
Concorde [37]	Code	https://github.com/jvkersch/pyconcorde	BSD 3-Clause License
LKH3 [3]	Code	http://webhotel4.ruc.dk/~keld/research/LKH-3/	Available for academic research use
HGS [4]	Code	https://github.com/chkwon/PyHygese	MIT License
GLOP [39]	Code	https://github.com/henry-yeh/GLOP	MIT License
POMO [18]	Code	https://github.com/yd-kwon/POMO/tree/master/NEW_py_ver	MIT License
ELG [26]	Code	https://github.com/gaocr/ELG	MIT License
Omni_VRP [38]	Code	https://github.com/RoyalSkye/Omni-VRP	MIT License
INVIT [28]	Code	https://github.com/Kasumigaoka-Utaha/INVIT	MIT License
LEHD [9]	Code	https://github.com/CIAM-Group/NCO_code/tree/main/single_objective/LEHD	Available for academic research use
BQ [10]	Code	https://github.com/naver/bq-nco	Available for any non-commercial use CC BY-NC-SA 4.0 license
Cross-distribution TSPs[28]	Dataset	https://github.com/Kasumigaoka-Utaha/INVIT	MIT License
Cross-distribution CVRPs[28]	Dataset	https://github.com/Kasumigaoka-Utaha/INVIT	MIT License
TSPLIB [29]	Dataset	http://comopt.ifii.uni-heidelberg.de/software/TSPLIB95/	Available for any non-commercial use
CVRPLIB Set-XXL [35]	Dataset	http://vrp.galgos.inf.puc-rio.br/index.php/en/	Available for academic research use

We list the used existing codes and datasets in Table 18, and all of them are open-sourced resources for academic usage.

N Broader Impacts

This paper presents work whose goal is to advance the field of Neural Combinatorial Optimization. We believe the proposed L2R framework is valuable for promoting the further development of the field, such as improved efficiency in solving large-scale combinatorial optimization problems. This work can inspire follow-up works to explore more efficient neural methods for solving large-scale routing problems. The proposed method has no potential negative societal impacts that we feel must be specifically highlighted.

NeurIPS Paper Checklist

1. Claims

Question: Do the main claims made in the abstract and introduction accurately reflect the paper's contributions and scope?

Answer: [\[Yes\]](#)

Justification: Yes, the abstract and introduction accurately reflect the paper's contributions and scope by presenting a novel learning-based search space reduction framework, significantly reducing the search space while maintaining solution quality of large-scale routing instances. These accurately reflect the paper's scope and are substantiated by the subsequent results, indicating their generalizability.

Guidelines:

- The answer NA means that the abstract and introduction do not include the claims made in the paper.
- The abstract and/or introduction should clearly state the claims made, including the contributions made in the paper and important assumptions and limitations. A No or NA answer to this question will not be perceived well by the reviewers.
- The claims made should match theoretical and experimental results, and reflect how much the results can be expected to generalize to other settings.
- It is fine to include aspirational goals as motivation as long as it is clear that these goals are not attained by the paper.

2. Limitations

Question: Does the paper discuss the limitations of the work performed by the authors?

Answer: [\[Yes\]](#)

Justification: Yes, this paper discusses the limitations of the proposed L2R framework in Section 5.

Guidelines:

- The answer NA means that the paper has no limitation while the answer No means that the paper has limitations, but those are not discussed in the paper.
- The authors are encouraged to create a separate "Limitations" section in their paper.
- The paper should point out any strong assumptions and how robust the results are to violations of these assumptions (e.g., independence assumptions, noiseless settings, model well-specification, asymptotic approximations only holding locally). The authors should reflect on how these assumptions might be violated in practice and what the implications would be.
- The authors should reflect on the scope of the claims made, e.g., if the approach was only tested on a few datasets or with a few runs. In general, empirical results often depend on implicit assumptions, which should be articulated.
- The authors should reflect on the factors that influence the performance of the approach. For example, a facial recognition algorithm may perform poorly when image resolution is low or images are taken in low lighting. Or a speech-to-text system might not be used reliably to provide closed captions for online lectures because it fails to handle technical jargon.
- The authors should discuss the computational efficiency of the proposed algorithms and how they scale with dataset size.
- If applicable, the authors should discuss possible limitations of their approach to address problems of privacy and fairness.
- While the authors might fear that complete honesty about limitations might be used by reviewers as grounds for rejection, a worse outcome might be that reviewers discover limitations that aren't acknowledged in the paper. The authors should use their best judgment and recognize that individual actions in favor of transparency play an important role in developing norms that preserve the integrity of the community. Reviewers will be specifically instructed to not penalize honesty concerning limitations.

3. Theory assumptions and proofs

Question: For each theoretical result, does the paper provide the full set of assumptions and a complete (and correct) proof?

Answer: [NA]

Justification: The results presented by this paper are all experimental. That is, the paper does not include theoretical results, and therefore, there are no assumptions or proofs to provide.

Guidelines:

- The answer NA means that the paper does not include theoretical results.
- All the theorems, formulas, and proofs in the paper should be numbered and cross-referenced.
- All assumptions should be clearly stated or referenced in the statement of any theorems.
- The proofs can either appear in the main paper or the supplemental material, but if they appear in the supplemental material, the authors are encouraged to provide a short proof sketch to provide intuition.
- Inversely, any informal proof provided in the core of the paper should be complemented by formal proofs provided in appendix or supplemental material.
- Theorems and Lemmas that the proof relies upon should be properly referenced.

4. Experimental result reproducibility

Question: Does the paper fully disclose all the information needed to reproduce the main experimental results of the paper to the extent that it affects the main claims and/or conclusions of the paper (regardless of whether the code and data are provided or not)?

Answer: [Yes]

Justification: Yes, this paper fully discloses all necessary details for reproducing experimental results. This includes comprehensive descriptions of: model architecture (Section 3, Appendix E, and Appendix F), dataset descriptions (Section 4), parameter settings (Appendix I), and experimental setups (Appendix H), ensuring that the results can be independently verified.

Guidelines:

- The answer NA means that the paper does not include experiments.
- If the paper includes experiments, a No answer to this question will not be perceived well by the reviewers: Making the paper reproducible is important, regardless of whether the code and data are provided or not.
- If the contribution is a dataset and/or model, the authors should describe the steps taken to make their results reproducible or verifiable.
- Depending on the contribution, reproducibility can be accomplished in various ways. For example, if the contribution is a novel architecture, describing the architecture fully might suffice, or if the contribution is a specific model and empirical evaluation, it may be necessary to either make it possible for others to replicate the model with the same dataset, or provide access to the model. In general, releasing code and data is often one good way to accomplish this, but reproducibility can also be provided via detailed instructions for how to replicate the results, access to a hosted model (e.g., in the case of a large language model), releasing of a model checkpoint, or other means that are appropriate to the research performed.
- While NeurIPS does not require releasing code, the conference does require all submissions to provide some reasonable avenue for reproducibility, which may depend on the nature of the contribution. For example
 - (a) If the contribution is primarily a new algorithm, the paper should make it clear how to reproduce that algorithm.
 - (b) If the contribution is primarily a new model architecture, the paper should describe the architecture clearly and fully.
 - (c) If the contribution is a new model (e.g., a large language model), then there should either be a way to access this model for reproducing the results or a way to reproduce the model (e.g., with an open-source dataset or instructions for how to construct the dataset).

(d) We recognize that reproducibility may be tricky in some cases, in which case authors are welcome to describe the particular way they provide for reproducibility. In the case of closed-source models, it may be that access to the model is limited in some way (e.g., to registered users), but it should be possible for other researchers to have some path to reproducing or verifying the results.

5. Open access to data and code

Question: Does the paper provide open access to the data and code, with sufficient instructions to faithfully reproduce the main experimental results, as described in supplemental material?

Answer: [No]

Justification: All our training code and pre-trained models will be open-sourced upon publication to ensure easy reproduction.

Guidelines:

- The answer NA means that paper does not include experiments requiring code.
- Please see the NeurIPS code and data submission guidelines (<https://nips.cc/public/guides/CodeSubmissionPolicy>) for more details.
- While we encourage the release of code and data, we understand that this might not be possible, so “No” is an acceptable answer. Papers cannot be rejected simply for not including code, unless this is central to the contribution (e.g., for a new open-source benchmark).
- The instructions should contain the exact command and environment needed to run to reproduce the results. See the NeurIPS code and data submission guidelines (<https://nips.cc/public/guides/CodeSubmissionPolicy>) for more details.
- The authors should provide instructions on data access and preparation, including how to access the raw data, preprocessed data, intermediate data, and generated data, etc.
- The authors should provide scripts to reproduce all experimental results for the new proposed method and baselines. If only a subset of experiments are reproducible, they should state which ones are omitted from the script and why.
- At submission time, to preserve anonymity, the authors should release anonymized versions (if applicable).
- Providing as much information as possible in supplemental material (appended to the paper) is recommended, but including URLs to data and code is permitted.

6. Experimental setting/details

Question: Does the paper specify all the training and test details (e.g., data splits, hyper-parameters, how they were chosen, type of optimizer, etc.) necessary to understand the results?

Answer: [Yes]

Justification: Yes, all necessary experimental settings and details are specified in Section 4, with full details in Appendix H and Appendix I, ensuring the experiments can be comprehensively understood.

Guidelines:

- The answer NA means that the paper does not include experiments.
- The experimental setting should be presented in the core of the paper to a level of detail that is necessary to appreciate the results and make sense of them.
- The full details can be provided either with the code, in appendix, or as supplemental material.

7. Experiment statistical significance

Question: Does the paper report error bars suitably and correctly defined or other appropriate information about the statistical significance of the experiments?

Answer: [No]

Justification: The paper does not report error bars or any other direct measures of statistical significance. In Neural Combinatorial Optimization (NCO), we usually use the gap (i.e., the difference from the optimal value) and solving time as two deterministic metrics to validate the reliability and robustness of the results.

Guidelines:

- The answer NA means that the paper does not include experiments.
- The authors should answer "Yes" if the results are accompanied by error bars, confidence intervals, or statistical significance tests, at least for the experiments that support the main claims of the paper.
- The factors of variability that the error bars are capturing should be clearly stated (for example, train/test split, initialization, random drawing of some parameter, or overall run with given experimental conditions).
- The method for calculating the error bars should be explained (closed form formula, call to a library function, bootstrap, etc.)
- The assumptions made should be given (e.g., Normally distributed errors).
- It should be clear whether the error bar is the standard deviation or the standard error of the mean.
- It is OK to report 1-sigma error bars, but one should state it. The authors should preferably report a 2-sigma error bar than state that they have a 96% CI, if the hypothesis of Normality of errors is not verified.
- For asymmetric distributions, the authors should be careful not to show in tables or figures symmetric error bars that would yield results that are out of range (e.g. negative error rates).
- If error bars are reported in tables or plots, The authors should explain in the text how they were calculated and reference the corresponding figures or tables in the text.

8. Experiments compute resources

Question: For each experiment, does the paper provide sufficient information on the computer resources (type of compute workers, memory, time of execution) needed to reproduce the experiments?

Answer: [Yes]

Justification: Yes, the paper provides detailed information on the compute resources used for the experiments in Section 4, including the type of compute workers, memory specifications, and execution time, ensuring that the experiments can be accurately reproduced. More specifically, we train and test all experiments using a single NVIDIA GeForce RTX 3090 GPU with 24GB of memory.

Guidelines:

- The answer NA means that the paper does not include experiments.
- The paper should indicate the type of compute workers CPU or GPU, internal cluster, or cloud provider, including relevant memory and storage.
- The paper should provide the amount of compute required for each of the individual experimental runs as well as estimate the total compute.
- The paper should disclose whether the full research project required more compute than the experiments reported in the paper (e.g., preliminary or failed experiments that didn't make it into the paper).

9. Code of ethics

Question: Does the research conducted in the paper conform, in every respect, with the NeurIPS Code of Ethics <https://neurips.cc/public/EthicsGuidelines>?

Answer: [Yes]

Justification: Yes, the research conducted in the paper conforms with the NeurIPS Code of Ethics. Its principles and guidelines were carefully considered and adhered to throughout this study.

Guidelines:

- The answer NA means that the authors have not reviewed the NeurIPS Code of Ethics.
- If the authors answer No, they should explain the special circumstances that require a deviation from the Code of Ethics.
- The authors should make sure to preserve anonymity (e.g., if there is a special consideration due to laws or regulations in their jurisdiction).

10. Broader impacts

Question: Does the paper discuss both potential positive societal impacts and negative societal impacts of the work performed?

Answer: [Yes]

Justification: Yes, Appendix N details the potential positive societal impacts of this work. And the proposed method has no potential negative societal impacts that we feel must be specifically highlighted.

Guidelines:

- The answer NA means that there is no societal impact of the work performed.
- If the authors answer NA or No, they should explain why their work has no societal impact or why the paper does not address societal impact.
- Examples of negative societal impacts include potential malicious or unintended uses (e.g., disinformation, generating fake profiles, surveillance), fairness considerations (e.g., deployment of technologies that could make decisions that unfairly impact specific groups), privacy considerations, and security considerations.
- The conference expects that many papers will be foundational research and not tied to particular applications, let alone deployments. However, if there is a direct path to any negative applications, the authors should point it out. For example, it is legitimate to point out that an improvement in the quality of generative models could be used to generate deepfakes for disinformation. On the other hand, it is not needed to point out that a generic algorithm for optimizing neural networks could enable people to train models that generate Deepfakes faster.
- The authors should consider possible harms that could arise when the technology is being used as intended and functioning correctly, harms that could arise when the technology is being used as intended but gives incorrect results, and harms following from (intentional or unintentional) misuse of the technology.
- If there are negative societal impacts, the authors could also discuss possible mitigation strategies (e.g., gated release of models, providing defenses in addition to attacks, mechanisms for monitoring misuse, mechanisms to monitor how a system learns from feedback over time, improving the efficiency and accessibility of ML).

11. Safeguards

Question: Does the paper describe safeguards that have been put in place for responsible release of data or models that have a high risk for misuse (e.g., pretrained language models, image generators, or scraped datasets)?

Answer: [NA]

Justification: The paper poses no such risks.

Guidelines:

- The answer NA means that the paper poses no such risks.
- Released models that have a high risk for misuse or dual-use should be released with necessary safeguards to allow for controlled use of the model, for example by requiring that users adhere to usage guidelines or restrictions to access the model or implementing safety filters.
- Datasets that have been scraped from the Internet could pose safety risks. The authors should describe how they avoided releasing unsafe images.
- We recognize that providing effective safeguards is challenging, and many papers do not require this, but we encourage authors to take this into account and make a best faith effort.

12. Licenses for existing assets

Question: Are the creators or original owners of assets (e.g., code, data, models), used in the paper, properly credited and are the license and terms of use explicitly mentioned and properly respected?

Answer: [Yes]

Justification: Yes, all existing assets are properly credited to their original creators. Their respective licenses and terms of use are explicitly stated and have been respected. Full details and attribution for each asset are provided in Appendix M.

Guidelines:

- The answer NA means that the paper does not use existing assets.
- The authors should cite the original paper that produced the code package or dataset.
- The authors should state which version of the asset is used and, if possible, include a URL.
- The name of the license (e.g., CC-BY 4.0) should be included for each asset.
- For scraped data from a particular source (e.g., website), the copyright and terms of service of that source should be provided.
- If assets are released, the license, copyright information, and terms of use in the package should be provided. For popular datasets, paperswithcode.com/datasets has curated licenses for some datasets. Their licensing guide can help determine the license of a dataset.
- For existing datasets that are re-packaged, both the original license and the license of the derived asset (if it has changed) should be provided.
- If this information is not available online, the authors are encouraged to reach out to the asset's creators.

13. New assets

Question: Are new assets introduced in the paper well documented and is the documentation provided alongside the assets?

Answer: [NA]

Justification: This paper does not introduce any new assets. All assets used, such as datasets, code, and pre-trained models, are sourced from prior, published research or are based on established techniques, all of which are appropriately cited. All our training code and pre-trained models will be open-sourced upon publication to ensure easy reproduction.

Guidelines:

- The answer NA means that the paper does not release new assets.
- Researchers should communicate the details of the dataset/code/model as part of their submissions via structured templates. This includes details about training, license, limitations, etc.
- The paper should discuss whether and how consent was obtained from people whose asset is used.
- At submission time, remember to anonymize your assets (if applicable). You can either create an anonymized URL or include an anonymized zip file.

14. Crowdsourcing and research with human subjects

Question: For crowdsourcing experiments and research with human subjects, does the paper include the full text of instructions given to participants and screenshots, if applicable, as well as details about compensation (if any)?

Answer: [NA]

Justification: The paper does not involve crowdsourcing nor research with human subjects.

Guidelines:

- The answer NA means that the paper does not involve crowdsourcing nor research with human subjects.
- Including this information in the supplemental material is fine, but if the main contribution of the paper involves human subjects, then as much detail as possible should be included in the main paper.

- According to the NeurIPS Code of Ethics, workers involved in data collection, curation, or other labor should be paid at least the minimum wage in the country of the data collector.

15. Institutional review board (IRB) approvals or equivalent for research with human subjects

Question: Does the paper describe potential risks incurred by study participants, whether such risks were disclosed to the subjects, and whether Institutional Review Board (IRB) approvals (or an equivalent approval/review based on the requirements of your country or institution) were obtained?

Answer: [NA]

Justification: The paper does not involve crowdsourcing nor research with human subjects.

Guidelines:

- The answer NA means that the paper does not involve crowdsourcing nor research with human subjects.
- Depending on the country in which research is conducted, IRB approval (or equivalent) may be required for any human subjects research. If you obtained IRB approval, you should clearly state this in the paper.
- We recognize that the procedures for this may vary significantly between institutions and locations, and we expect authors to adhere to the NeurIPS Code of Ethics and the guidelines for their institution.
- For initial submissions, do not include any information that would break anonymity (if applicable), such as the institution conducting the review.

16. Declaration of LLM usage

Question: Does the paper describe the usage of LLMs if it is an important, original, or non-standard component of the core methods in this research? Note that if the LLM is used only for writing, editing, or formatting purposes and does not impact the core methodology, scientific rigorousness, or originality of the research, declaration is not required.

Answer: [NA]

Justification: The use of LLMs is confined to assisting with the writing and editing of the manuscript. LLMs are not used as an important, original, or non-standard component of the core research methods described in this paper.

Guidelines:

- The answer NA means that the core method development in this research does not involve LLMs as any important, original, or non-standard components.
- Please refer to our LLM policy (<https://neurips.cc/Conferences/2025/LLM>) for what should or should not be described.